Optical Limiter Based on Phase Change Material

Dan Guo

A thesis

submitted in partial fulfillment of the

requirements for the degree of

Master of Science in Electrical Engineering

University of Washington

2017

Committee:

Arka Majumdar

Lih Lin

Program Authorized to Offer Degree:

Electrical Engineering

University of Washington

Abstract

Optical Limiter Based on Phase Change Material

Dan Guo

Chair of the Supervisory Committee:
Dr. Arka Majumdar
Department of Electrical Engineering

Optical limiter is a potential optical device to limit input light intensity to protect optical sensitive devices. It has a large transmissivity (T) when the input intensity is low and a low transmissivity when the input intensity exceeds a certain level. Thus, there is a nonlinear transition between the high and low level of power transmittance. In this project, we proposed a design of an optical limiter by utilizing phase change material. Phase change material has a large contrast in optical properties between its amorphous and crystalline state which could be used in an optical limiter as its High-T state and Low-T state respectively. The phase changes from one state to the other state according to the input intensity within a very narrow range of the input power. Such significant change allows design of a well performing optical limiter and has promising future applications.

TABLE OF CONTENTS

List of Figures

Chapter 1. Introduction

Optical limiters are devices that have a high transmittance (T) when their input light intensity is low and have a decreasing transmittance within a particular range when the input power increases. As a result, the optical limiter's transmittance stays at a relatively low level when the input intensity is beyond a certain level. Therefore, under the illumination with relatively large input intensity, an optical limiter is able to block most of the incident light due to its low-T property. Hence optical limiters can be used to protect human eyes and other tissues or organs from laser injury. Optical limiters also protect equipments, and instruments that are sensitive to high optical radiation. In addition, optical limiters can potentially find usage in military defense devices such as fighting against those laser weapons not only in science fictions and movies but also under current research and developments by many governments or military companies. In a nutshell, optical limiters are promising optical devices that have wild varieties of applications in daily lives, manufactural industries, products development, academic researches and even in national security areas.

With the radiation limiting property, the transmittance of an optical limiter must have a nonlinear relation to the light that is injected into the device. This requires the material inside an optical limiter to have increasingly large photon absorption as a function of the input light power, especially when the input power is around a certain point, which is also known as the switching threshold power P_{th}. To perform this nonlinear relation, many of the current research works regarding optical limiters chose materials whose crystal structure will be damaged at a certain threshold power due to the device's overheating or dielectric breakdown[1]. Then materials' optical properties would be largely altered and have low transmittance to largely block the input light though the device. Unfortunately, the device itself will be irreversibly damaged and cannot

reverted back to its initial state. Another severe problem is that many of the non-linear materials do not exhibit a large change in optical properties to result significant differences on the transmissivity of the device. Hence, using conventional non-linear materials, it is difficult to lower the transmittance sufficiently to limit the input power. Hence, in this thesis, we utilized phase change material as our nonlinear material. Besides nonlinear material, in an optical limiter, it was proposed to use a planar microcavity or a F-P resonator by some groups[2-6] so the transmittance of the device becomes intensity dependent due to the resonance of the device shifts as a function of the input intensity. More importantly, a cavity works as an amplifier of the light power inside the device and makes it easier for an optical limiter to reach the functional region. Once the input light intensity is strong enough to drive the device beyond certain level, the resonance shifts significantly so that the transmittance of cavity changes dramatically from high to low. As a result, the input light is able to be successfully blocked.

In this thesis, we demonstrated a design of an optical limiter. As shown in Figure 1, besides using two DBRs to form a F-P cavity[1], we chose phase change material, GST specifically, between two

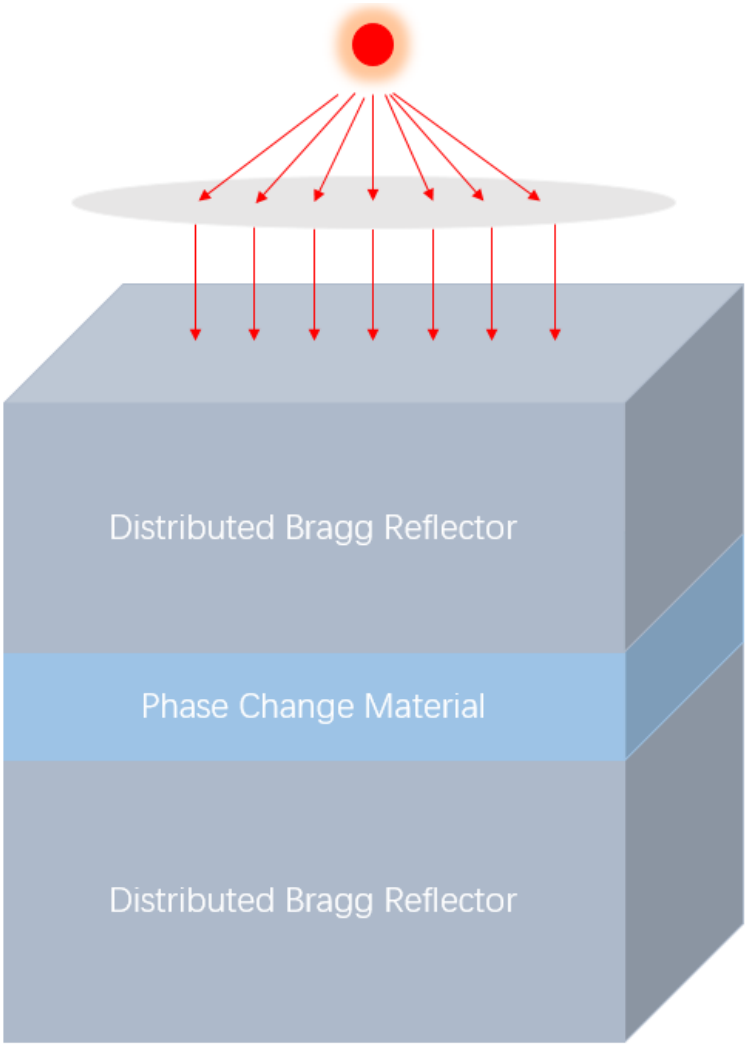

Figure 1 A basic schematic design of the optical limiter in our work

DBR mirrors to form a planar microcavity. Therefore, the transmittance of the device can be determined and tuned more efficiently by not only the dimensional size of the cavity but also the refractive index of its medium. Also, the cavity's resonance can be determined by many factors such as the device size, the refractive index of the materials we utilized, and of course, the input light intensity. Once the device structure and size is well designed for this optical limiter, the transmissivity of the limiter will be a function of the light power flows in and the wavelength of the input light. Hopefully, at low input intensity, the transmittance of the limiter is large so that light passes through. On the contrary, when the input intensity goes up, the temperature of the cavity increases drastically so that the GST switches from one state(amorphous) to the other(crystalline) state as it exceeds the crystallization temperature. As the result, the T of the device drops dramatically and the input light barely passes.

We will demonstrate the design of our optical limiter in this thesis and discuss the simulation results as well as several performance calculations regarding this device. This optical limiter was designed for an input light specifically with a center wavelength at 1550nm and the cavity resonance was set at that wavelength. First, we performed simulation by using COMSOL, to calculate the temperature distribution inside the cavity and the state of the GST change process inside the cavity. Based on the results of the thermal distribution simulation, we made several assumptions regarding the phase transition process of the GST. We also established a static modeling to understand the transmittance of the limiter as a function of wavelength under certain states. Then we will show how the T changes as a function of the power absorbed by the cavity P_{abs}. Analytical and dynamic models were also demonstrated in our work to obtain simulation results about the dynamic relation between the absorption power and the input power and what impacts they would have on the parameters of the GST cavity as well as the output power of the

device. Based on our design and the simulation results, we will demonstrate this optical limiter has a successful light limiting mechanism and is very promising in future actual applications as a method of optical protection.

This paper is divided into several sections. At first, we are going to introduce the general motivation of this work and some potential applications. The reasons of using a phase change material and Distributed Bragg Reflectors will be involved in this section. Then we will introduce the backgrounds of this optical limiter and some theoretical principles behind the design which will include the properties of a Distributed Bragg Reflector, a F-P cavity and phase change materials, especially GST. The third part is about the simulation and performance calculations of our design for an optical limiter, in which we will discuss the assumptions we have made in our models and the simulation results based on each assumption. This part contains three sub-topics: thermal distribution, static modeling and dynamic modeling. According to these models, we will also analyze the reasonability of these assumptions and discuss the results of the simulations. Finally, we summarize the work in this thesis and discuss our current progress on the actual fabrication and the experiment of a real optical limiter. In addition, we will also analyze how the experiment results would probably affect our simulation and what our future works would be.

Chapter 2. Motivation

2.1 Optical Limiter

Laser and its related applications have long been used into our life for decades. The basic principle behind this half-century-old invention is a significant amplification on light intensity. Laser devices are in a great many of usages to make life easier in almost every aspect of human's life. For instance, together with artificial satellites, it is applied to achieve telecommunication between two remote points on earth that are thousands of miles away from each other or even between satellites in the outer space[7]. Lasers are used for medical treatments to conduct surgeries or to cure disease or illness with human skin or other tissues for a long time[8, 9]. The applications of laser still include but are not limited to industrial manufactory, product development, public entertainment and even military weapons[10-12]. Additionally, at the very frontier of current researches on optical/photonic engineering, laser is playing a significant role in helping scientists explore the world of unknown and have a better understanding of this universe we live in[13, 14].

On the contrary, however, laser could be potentially hazardous due to its extremely high intensity. Laser has a particularly outstanding property of light convergence and low scattering that both result a very small light spot on its target. Hence a laser could introduce considerably high intensity even for one with a relatively low power. For instance, the heat a laser generates can easily cause thermal damage or burn on human tissues as long as it is strong enough to lead to protein denaturation[15]. Particularly, sufficiently powerful laser will penetrate eyeballs and result a high probability of cataracts or burn injuries[16]. For optically sensitive devices, either in the use of industries or researches, such as photon detectors, photonic integrated circuits or optical resonator, they may suffer from a great risk of being damaged by a sudden uproar of laser illumination when the circumstances of the device are not properly controlled. To make matters

worse, strong and powerful lasers under researches and experiments for military purposes can produce temporary or even permanent damage to either military targets or civilian objects[17]. Such lethal laser weapons will put civilian lives and objects under grave threats if they are in the wrong hands.

To prevent human beings, devices, objects from being damaged under the exposure of laser radiation and other kinds of light amplifiers, there is a great demand to have a novel device with a light limiting function. Naturally, the solution is optical limiter. As shown in Figure 2a, a typical optical limiter will let the light pass when its intensity is too weak to hurt humans' health, electronic devices, photodetectors or any other objects we want to protect. As increasing the intensity of input light, the optical limiter starts to block light when it exceeds a certain limiting threshold and the light passed through the device will be largely reduced or, at least, the increment of the passing light will decrease dramatically.

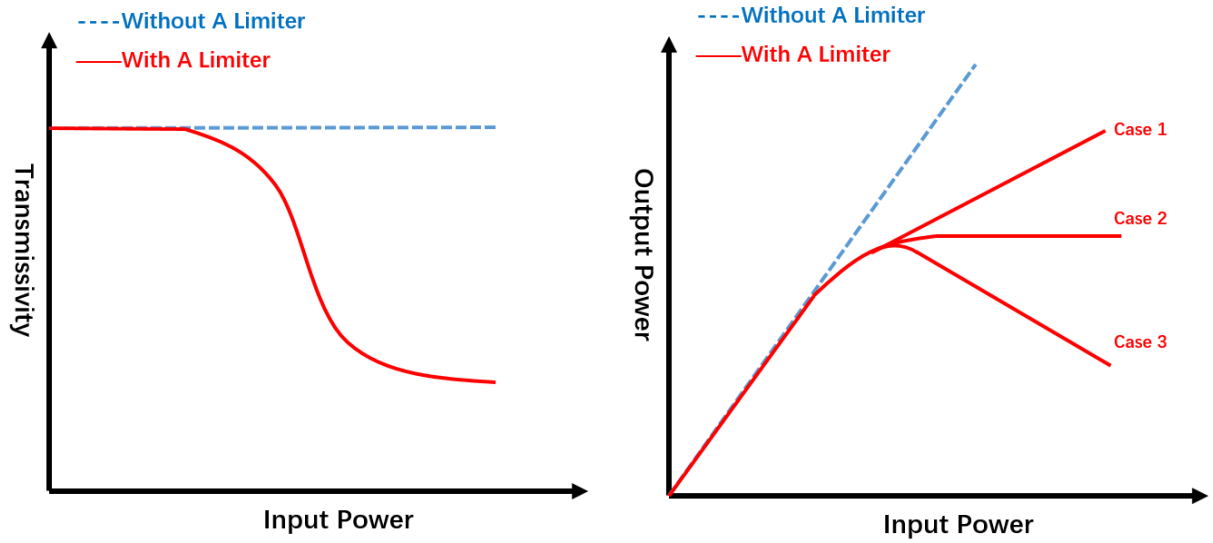

Figure 2a &2b The transmissivity and output power in an optical limiter

Figure 2b demonstrates three possible outcomes of the relation between the output power and the input power of an optical limiter. In an optical limiter, the output power will initially go up with the increasing of the input power in its high-T region when the input intensity is low. After

that region, the optical limiter will enter into its low-T area after certain level of the input power. As the input power goes beyond this value, the first possible case of the output power could be a decrease while input power is increasing. This happens if the limiter has a significant light limiting effect in this region and introduces a drastic decrease on the transmissivity of the device. Hence it leads a negative relation between the input and output power. Another case could be that the output power stays at a somewhat stationary level regardless of the input power as long as it is higher than a typical value. When the input power is in the interval that the T goes down, two factors will affect the output power: 1) the increase of the input power that has a potential to increase the output power and 2) the decrease of the transmissivity which introduces an inclination of limiting the increase of the output power. If both of the factors work just fine to cancel out the effect of each other, the total output of the device is likely to be stable in a certain range of the input power. In the third scenario, if the decrease of the transmissivity is too weak to completely cancel out the effect by increasing the input power, the total output power will probably have a positive relation with the input power. It will increase still as the increase of the input power, yet at a slower pace comparing to the initial increase. This is most likely to happen when the device has already been in its low-T area and there is not too much room for a further decrease on the power transmittance. As the result, the output power of the optical limiter will increase according to the increase of the input power but the pace of this increment should be smaller than that at the initial high-T level of the device.

Currently, most of existing optical limiters adopt nonlinear optical materials to achieve such light limiting effect. Under large light irradiation, these materials become opaque when light intensity reaches their light limiting threshold due to two-photon absorption[18, 19], nonlinear-optical energy regulation[20], broadband saturable absorption[21] and other light limiting

factors[22-24]. Most of these nonlinear materials, however, may suffer from an irreversible damage under large irradiation exposure because of dielectric breakdown and overheating. One possible solution is to utilize photonic microcavity with a low-loss nonlinear material. These limiters can block the light passing through because when the input intensity is strong enough to generate a shift on the cavity resonance. Hence, the transmittance of the input light at its original resonating wavelength shall go down. As a result, the light passing through the device is blocked when its intensity is above a certain level, which is also known as the limiting threshold. Nevertheless, this effect requires a dramatic resonance shift at the high-level of input intensity. Otherwise the change on the transmittance would be too small to have a significant impact on the output light.

2.2 Phase Change Material and Distributed Bragg Reflector

As a possible solution to get rid of the disadvantages of previous works on optical limiter, we proposed a solution by using optical limiter based on phase change materials. Phase change materials typically have two states, an amorphous state with randomly located atoms in its bulk and a crystalline state with periodic lattice. These two considerably different molecular structures within a single solid state material make it possible to have two largely different optical characters, especially the transmissivity, under different conditions if the device is properly designed. And these two states are switchable among each other at certain circumstances. Therefore, it is feasible for a such device with phase change material to transfer between a high-T device and a low-T device. For most phase change materials, the phase transition happens based on the temperature of the material. Therefore, for an optical limiter, the state of material in it will be totally determined by how much light power flows into the device. In recent years, phase change materials, such as

GST has generated strong interest in the photonics community, for the possibility of large change in the refractive index[25-28].

Besides phase change material, we also adopted optical microcavity in our device. By using a microcavity, a part of the incident light will travel back and forth inside the cavity which makes it easier for the material inside the cavity to absorb the power. Therefore, for a phase change material inside a cavity, the power that is actually needed to heat it up to its phase changing temperature should be lower than that with no cavity structure. And even at a relatively low input intensity, an optical limiter is able to transfer from its high-T state to low-T state and becomes functional to limit the input intensity. This feature makes a great potential application for such limiter in protecting photon sensitive devices such as photon detectors, photonic integrated circuits and some light subtle microchips.

Therefore, by utilizing both a plane microcavity and phase change material, one could obtain the best solution to have a reversible optical limiter that is functional at a relatively low range of input light intensity. It could be extremely useful for an optical limiter to block a large proportion of the incident light as long as the input intensity goes beyond the limiting threshold that makes the phase change material switch from one state to the other. The significant changes on the molecular structure actually have two contributions. First, the final state of a phase change material has a much greater optical loss than that at the initial state. Secondly, the change of its state also introduces a dramatic shift on the resonance of the microcavity. If the input light is at the resonance wavelength of the cavity, a large resonance shift is very likely to reduce the transmissivity of the device as well. When the input intensity goes below the threshold, then we could reset the phase change material back to its previous state that has a high transmittance. We are also able to alter the related parameters, such as the thickness of each layer of the device and the categories of phase

change materials to tune the resonance of the cavity to change the light limiting power threshold for various protecting targets. Hence, as a result, this optical limiter has an excellent potential in applications as a protecting and defensing device in very wild areas such as medicine, photonic engineering, health care, manufacturing industry, defense and national security.

Chapter 3. Backgrounds

As we mentioned above, there are two major components in this optical limiter, a plane microcavity and a layer of phase change material. Specifically, we utilized two identical Distributed Bragg Reflectors (DBRs) sitting symmetrically against each other to form a Fabry-Parot (F-P) Cavity. The F-P cavity is then able to confine a large proportion of the input light's energy in its cavity and has a resonant wavelength that depends on the thickness and refractive indices of each layer of the DBRs as well as those of the dielectric medium in the cavity. Particularly, for the inner layer in the F-P cavity, we adopted GeSbTe (Germanium-Antimony-Tellurium or GST) as the phase change material for our device.

3.1 Fabry-Parot Cavity

A F-P Cavity, whose meat part was developed by Charles Fabry and Alfred Perot in 1899[29, 30], is shown in Figure 3a[31]. It consists two pairs of partially reflective mirrors that could be made of optical glass, semiconductors, dielectrics, organic compounds. These two mirrors are spaced symmetrically with their reflective surfaces facing against each other. In Figure 3b, for instance, suppose there is a light source outside of a F-P cavity and a light is shined into the cavity from the left mirror. There is a proportion of injected light going through the mirror though the other part of it will be reflected back to the space. Just consider the part that passes through the left mirror and ignore the reflected part. It propagates within the medium between the two mirrors and reaches at the inner surface of mirror on the right-hand side. The light then splits

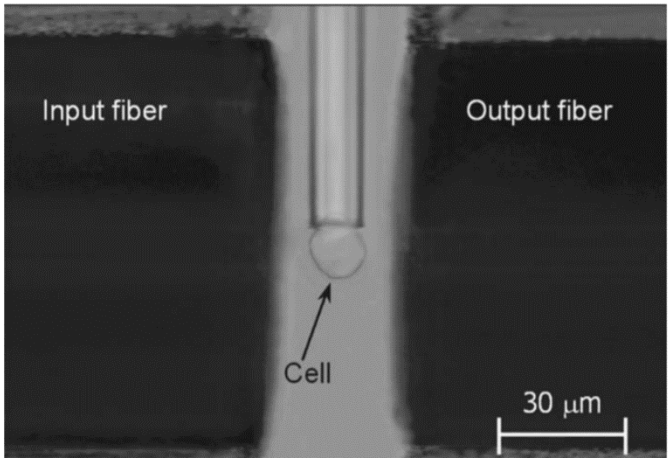

Figure 3a A photo picture of a Fabry-Perot cavity

apart. A small part goes through the right mirror towards the output port of the system while the other part will be reflected back into the medium and propagates towards the mirror on the left-hand side. Hence, as a result, the input light will bounce back and forth in the cavity while each time leaking a small portion of it out with different phases. For lights having a 2π (and any integer times of 2π) phase difference, they are now reaching the maximum of interference and forming a standing wave in the cavity which leads to the resonance of the cavity. The resonance wavelength of the cavity is determined by the geometry space between the two F-P mirrors, the reflectivity of them and the refractive index of the medium in the F-P cavity.

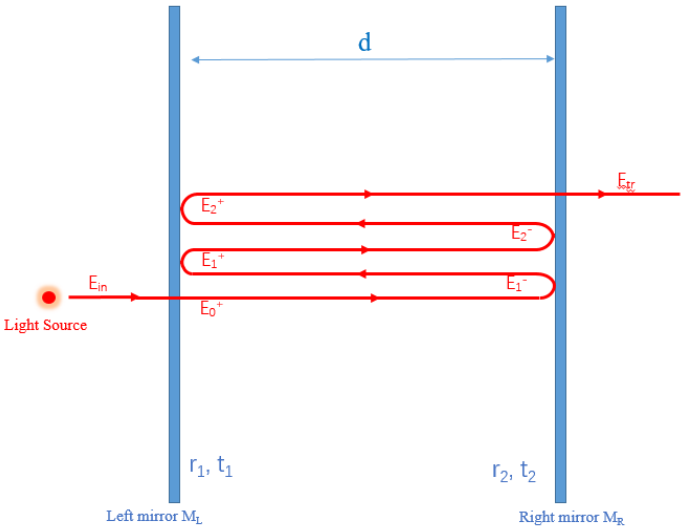

Figure 3b A general picture of a Fabry-Perot cavity

Assuming the E-fields that each time reach at the interface between the inner medium and the right mirror M_R are represented by E_0, E_1^+, E_2^+, …, and the input and transmitted E-fields are respectively E_{in} and E_{tr}. Then we have

$$\sum_{n=0}^{\infty} E_n^+ = E_0 + E_1^+ + E_2^+ + \ldots = E_0 + E_0 r_1 r_2 e^{-i\cdot 2\theta} + E_0\left(r_1 r_2 e^{-i\cdot 2\theta}\right)^2 + \ldots = \frac{E_0}{1 - r_1 r_2 e^{-i\cdot 2\theta}} \tag{1}$$

where r_1 and r_2 are the field reflection coefficients for the left mirror and the right mirror respectively. If we define t_1 and t_2 as the transmission coefficient for the left and the right mirror, we can also write the equations as the following.

$$E_0 = t_1 E_{in} \tag{2}$$

$$E_{tr} = t_2 e^{i\theta} \sum_{n=0}^{\infty} E_n^+ \tag{3}$$

Therefore, the proportion of input intensity to the transmitted intensity and the power transmittance can be represented as below.

$$\frac{E_{tr}}{E_{in}} = \frac{t_1 t_2 e^{-i\theta}}{1 - r_1 r_2 e^{-i\cdot 2\theta}} \tag{4}$$

$$T = \left|\frac{E_{tr}}{E_{in}}\right|^2 = \frac{t_1^2 t_2^2}{\left(1 - r_1 r_2 e^{-i\cdot 2\theta}\right)\left(1 - r_1 r_2 e^{i\cdot 2\theta}\right)} = \frac{\left(1 - R_1\right)\left(1 - R_2\right)}{\left(1 - \sqrt{R_1 R_2}\right)^2 + 4\sqrt{R_1 R_2}\sin^2\theta} \tag{5}$$

This is also referred as Airy Function[32] where R_1 and R_2 are the reflectivity of these two mirrors and θ is the phase shift caused by a single time of reflection where

$$\theta \equiv \frac{2n\pi}{\lambda} d \tag{6}$$

n is the refractive index of the medium in the cavity, d is the distance of the between the mirrors and λ is the wavelength of the input light in vacuum space.

Considering the equation (5) and (6) together, it would not be too hard to find the relation between the power transmittance and the wavelength and the size of the cavity. If we want to design a F-P cavity whose resonance is at 1550nm, for example, it would be straightforward for us to design a F-P cavity with a corresponding thickness of the inner medium as long as we get the refractive index of the material that we will utilize for the medium in the cavity.

3.2 Distributed Bragg Reflector

Distributed Bragg Reflector (DBR) is an optical structure formed by multilayers of alternating dielectric films. These two dielectric films have different refractive indices and periodically were stacked onto each other. Due to Bragg's Law[33] and the interference in dielectric films, as shown in Figure 4a, the reflected light from two interfaces of a dielectric film should have a constructive

light only when the equation nλ=2dsinθ is satisfied, where n is the refractive index of the dielectric film, d is the thickness of the film, λ is the wavelength of the light in vacuum, and θ is the incident angle. Specifically, at normal incidence, the Bragg Condition will be nλ=2d. For a two-layer system shown in Figure 4b, the reflective coefficient and the reflectivity are given by

$$r = \frac{n_1 - n_2}{n_1 + n_2} \tag{7}$$

$$R = |r|^2 \tag{8}$$

In a DBR, the structure could be treated as a periodically repeating two-layer dielectric system and the situation is a little bit more complicated than that of a two-layer system. A proportion of the incident light will be reflected at each interface between dielectric layers and the total reflection of a DBR is the superposition of all reflected light. As shown in Figure 4a, in order to get the highest reflection at center wavelength, the reflected light will have the best constructive reflection when the center wavelength is about 4 times of the thickness of each film. The approximate reflectivity of a DBR is given by equation (9)[34], where n_0, n_1, n_2, n_s are the refractive indices of air, first dielectric layer, second dielectric layer and the substrate, respectively. And N is the number of the repeating structure pairs in a DBR.

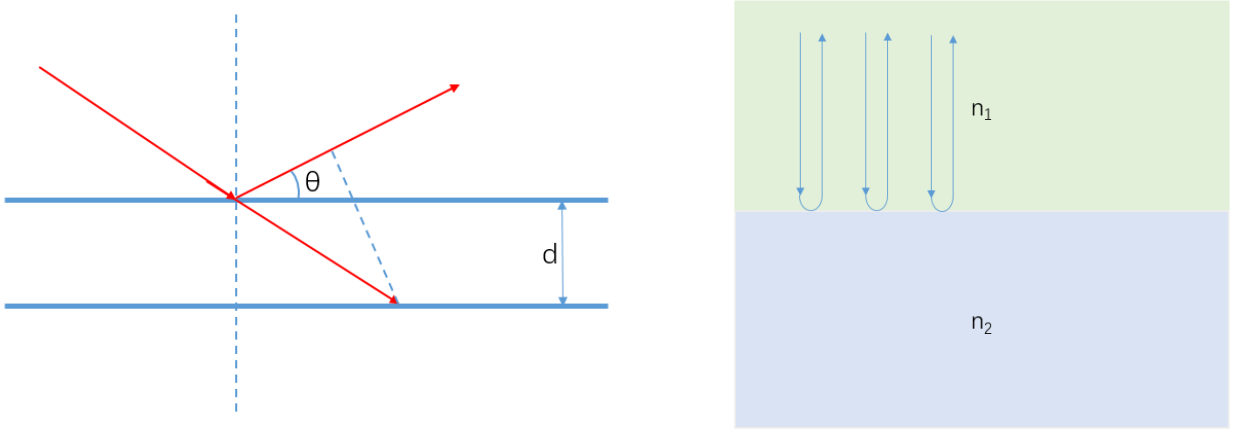

Figure 4 Bragg's Law (a) the reflection at the interfaces between dielectrics (b) reflection in a double layer structure with normal incidence

According to equation (9), we can tune the reflectivity by changing N and by altering the refractive indices n_1 and n_2, or selectively choosing the categories of the materials for each dielectric layer. And the frequency bandwidth Δf satisfies the equation (10)[35] where f_0 is the central frequency. Within the range of the frequency band, the input light signal has a relatively high the reflectivity given by the previous equation (9) and the transmission is low.

$$R = \left[\frac{n_0 (n_2)^{2N} - n_s (n_1)^{2N}}{n_0 (n_2)^{2N} + n_s (n_1)^{2N}} \right]^2 \tag{9}$$

$$\frac{\Delta f}{f_0} = \frac{4}{\pi} \arcsin\left(\frac{n_2 - n_1}{n_2 + n_1}\right) \tag{10}$$

Given equation (9) and (10), we are safe to say the contrast on the refractive index n_1 and n_2 has a numerically positive contribution to both the reflectivity and the frequency bandwidth of a DBR. At the same time, the more pairs of the repeating structure in a DBR which means greater N, the higher reflectivity it will result too. In an optical limiter, we desire to have a device with a large power transmittance at its initial state, thus a large T of the F-P cavity of the device. Based on the relation in equation (5), for a F-P cavity that the mirrors sitting on both sides of the cavity, $R_1=R_2=R_{eff}$, its transmissivity is given in equation (11) as below, where R_{eff} is the effective reflectivity of the DBR mirror[36]. We need to be very careful here because the reflectivity R of a single DBR is not the same as the effective reflectivity R_{eff} in the DBR mirror of a F-P cavity although they rise and drop simultaneously[36]. Hence, we incline to have a large reflectivity for the Distributed Bragg Reflector so that the F-P cavity will have a large power transmittance.

$$T_{FP} = \frac{(1 - R_{eff})^2}{(1 - R_{eff})^2 + 4R_{eff} \sin^2 \theta} \tag{11}$$

In terms of the design in our project, as shown in Figure 4c, in order to reach as large reflectivity as possible, we designed our DBR by using 6 pairs (we will demonstrate the reason in

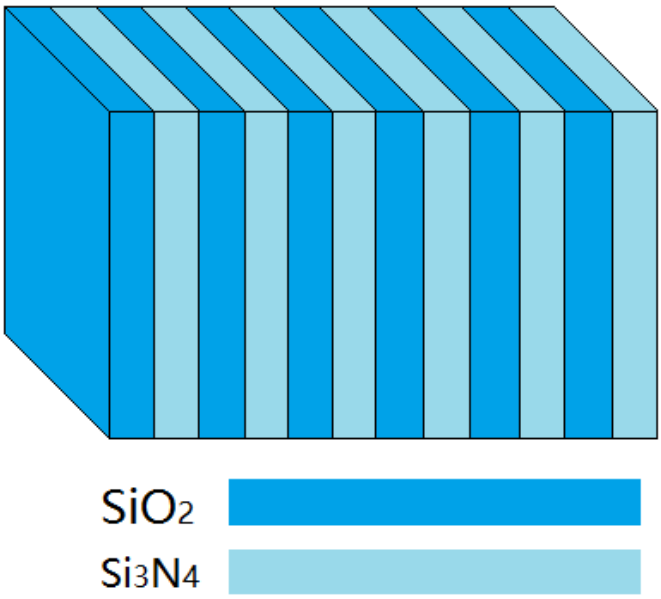

Figure 4c The design of the DBR in our work

the performance calculation section of the paper later) of alternating Silicon Nitride (Si_3N_4) layer and Silica layer (SiO_2) because they have a relatively large difference between their refractive indices. There are actually many other options for the materials we could use upon our DBR. For instance, the combination of silicon and silicon nitride has an even higher difference between their refractive indices than that between silica and silicon nitride. Nevertheless, silicon has a very strong two photon absorption that will introduce a significant loss for our device, and we had to discard that option. In order to build a constructive interference for this multilayer structure, these layers were designed to be as quarter-wavelength layers[37]. Considering the refractive indices of SiO_2 and Si_3N_4 are respectively 1.49 and 2.16 at 1550nm[38], the wavelength of the SiO_2 layer and the Si_3N_4 layer are respectively 260.0nm and 179.4nm.

Currently there are a lot of application regarding Distributed Bragg Reflectors, such as Vertical Cavity Surface Emitting Laser (VCSEL), photonic crystal fiber, fiber bragg grating[39]. For example, Figure 5 shows a schematic figure of a VCSEL. It has a similar structure to the optical limiter we designed though the purpose and function of these devices are actually way different from each other. It also contains a pair of DBR mirrors to form a cavity, in which sits a gain medium as the active region to amplify the input power and generate a high intensity output

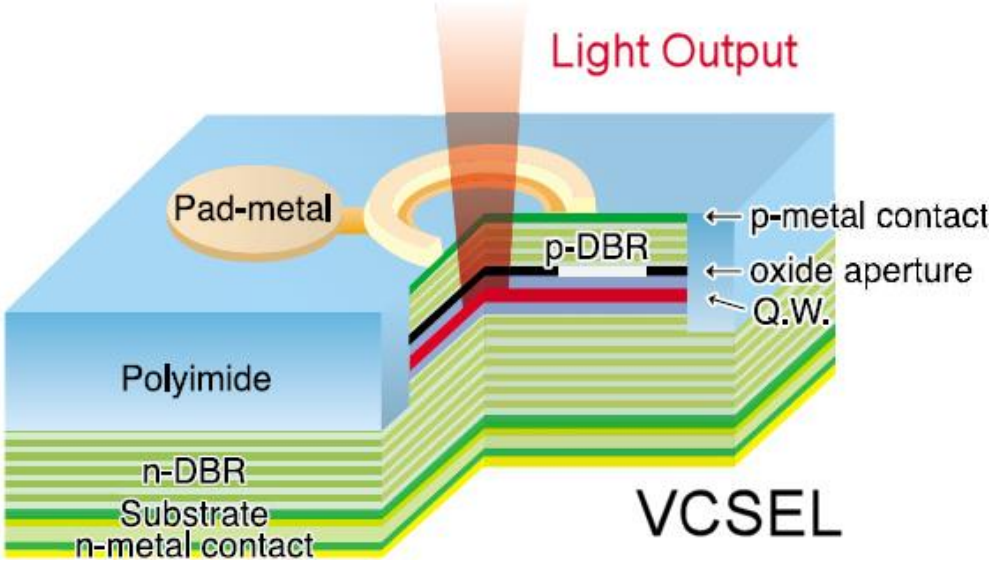

Figure 5 A schematic plot of a VCSEL

which is laser. While on the contrary, our purpose is to limit the input power when it is beyond a certain level. Therefore, we had to replace the active region in a VCSEL by phase change material that has a nonlinear absorption according to the power of the device's input light.

3.3 Phase Change Material

Phase change material is a promising material that triggered great interests in researches in the recent years though the mechanism of the phase transition process is still not clear. It has two distinguishable states: one is a crystalline phase with a relatively low resistivity and the other is an amorphous phase with a comparatively high resistivity. And these two phases can be reversibly switched the other phase state. More specifically, a phase change material has two physic temperature points, which are crystalline temperature and melt temperature respectively where the melt temperature is greater than the crystalline temperature ($T_{melt}>T_{crys}$).

The basic principle of phase changing can be briefly explained as following. Let's assume that the material is initially at its crystalline phase. When an input light pulse is applied to the material and the pulse generates a sharp increase of the material's temperature that excesses its melt temperature, the material is about to being melted when the temperature is beyond T_{melt}. Since

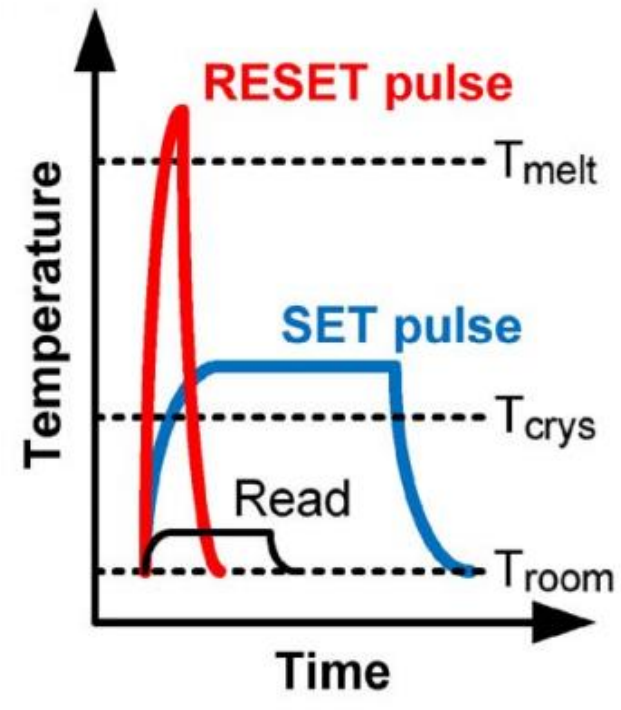

Figure 6 The temperatures that trigger phase transition of GST phase change memory

the light pulse only last for a very short of time, the melting material is then quenched rapidly, leaving its structure to be an amorphous state. For the process of the amorphous switching to the crystalline phase, a relative lower, but lasting longer light, for example CW light, is applied to the phase change material. PCM absorbs part of the energy of the light and it increases the material's temperature going beyond the crystalline temperature but lower than the melt temperature ($T_{melt}>T>T_{crys}$). Under this situation, the material with an amorphous phase begins to anneal and change gradually to crystallize into a state with high refractive index. Thus it is possible to switch the two distinct phases into each other. The relationship of temperature versus time is shown in Figure 6[40].

To design an optical limiter with phase change material, the prerequisites must be satisfied for the materials it utilizes. One of the most essential properties of the material is that the difference between its refractive indices at amorphous state and crystalline state has to be distinct, so that when the input light is applied, the variance in resonances of the device between the two states are remarkable. Typically, the low refractive index at amorphous state is often much lower than the high refractive at crystalline state. Another contributing feature of the phase change material is that its melting temperature and the crystalline temperature should be disparate enough. If not, the

input intensity to trigger the Set and/or the Reset process can be too narrow to tolerate possible perturbations in reality. That is to say, T_{melt} and T_{crys} have to be distinct enough so that there is room for pulse error. This is directly related to the stability of optical limiter devices.

Nevertheless, it should be pointed out that although the T_{melt} and T_{crys} are supposed to be distinct, it does not necessarily imply that either T_{melt} or T_{crys} has to be very high. Actually, taking the real applications into account, neither of them should excess the temperature limitation that would possibly make the F-P cavity and DBR fail.

It is a very popular adoption to use $Ge_2Sb_2Te_5$ (GST) or other doped GST compounds to fabricate current PCM[40-42]. And we as well chose GST in our work to design our optical limiter. Figure 7 shows the molecular structure of a GST in amorphous state and crystalline state respectively. The crystallization temperature of GST is about 400K and its melting temperature is around 900K[43].

In our design, a layer of GST was filled into the F-P cavity as its medium. Figure 8 demonstrates the refractive index, both the real part n and the imaginary part k, as a function of the wavelength of incident light. The imaginary part of the refractive index in amorphous state k_a

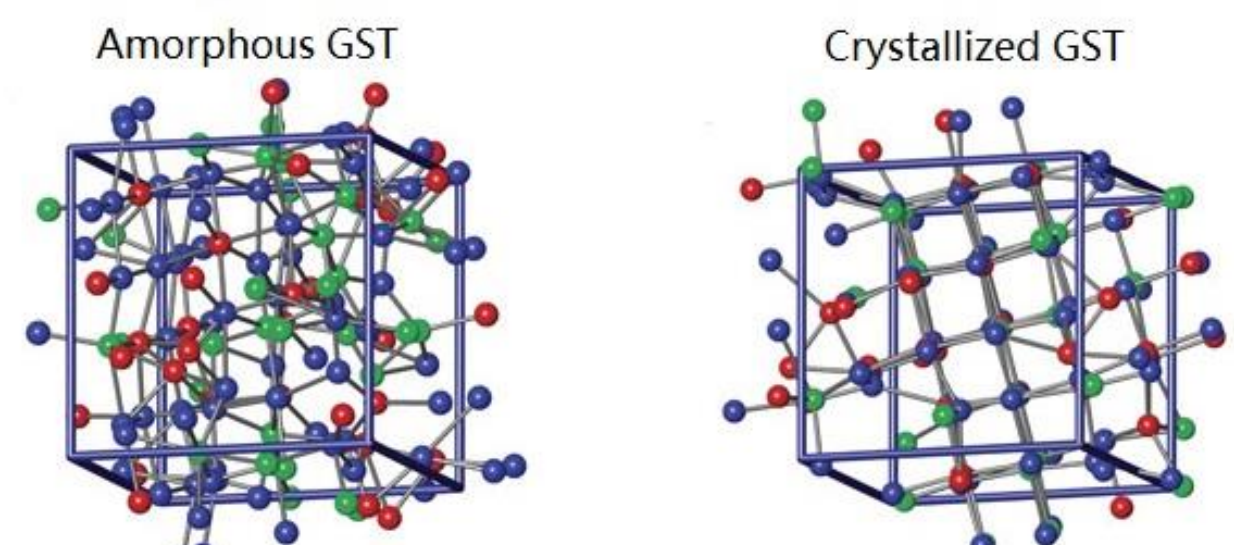

Figure 7 The molecular structures of a GST in both amorphous state and crystalline state

is basically smaller than that in crystalline state k_c in the entire wavelength range. This indicates that the GST layer suffers from greater loss in crystalline state than in amorphous state. When the input light is at low intensity, the transmittance of the optical limiter is supposed to be at high-level so the loss of the GST layer should be at low-level. Therefore, at the low-input intensity level, the GST should be in its amorphous state as the initial state.

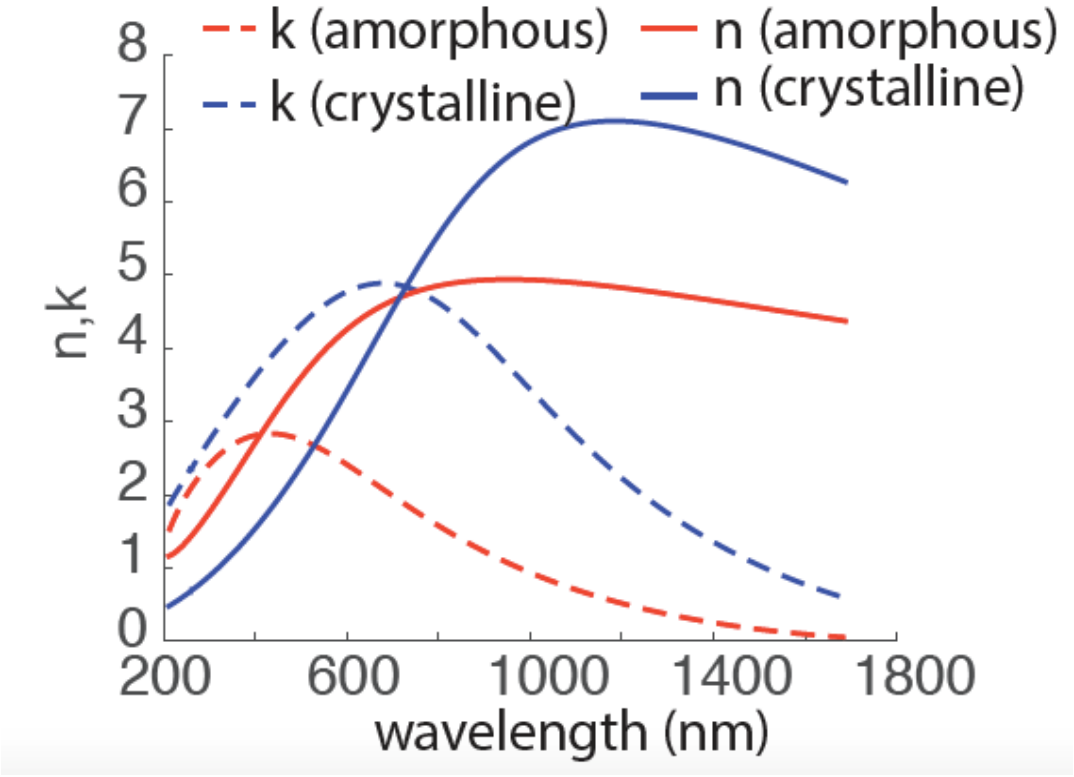

Figure 8 The refractive index of GST as a function of wavelength

For a well functional optical limiter, its transmissivity in the crystalline state of GST should be distinguishably higher than that in its amorphous state so that the limiter could have a great limiting effect on the input light. The refractive index of GST between these two states are very different. A distinct variance on the real part of refractive index will result a dramatic resonance shift in the cavity so that the power transmittance at the center wavelength will considerably drop. But we also need to be very careful to ensure this shift does not bring adjacent resonance modes of the cavity too close to the center wavelength. The imaginary part of the refractive index in

amorphous state should be a small value thus the device will not suffer from a large optical loss in amorphous state where the T is supposed to be high. The limiting effect caused by the change on the real part of the refractive index is much greater than that caused by the change on the imaginary part of the refractive index. It does not necessarily mean that the contrast between them has to be a lot higher, though a greater difference between the imaginary part of the refractive indices contributes to an even greater light limiting effect. According to Figure 8 (the measured data on GST in our lab), we believe the refractive index of GST can satisfy the requirements mentioned above in the infrared range so we basically consider infrared light in our work. Typically, we set 1550nm as the center wavelength of the input because 1550nm is a typical wavelength in applications about optical fiber communication. At 1550nm, the refractive index n_a and k_a at amorphous state are, respectively, n_a=4.51 and k_a=0.12 while those at crystalline state are respectively n_c=6.59 and k_c=0.89.

When the input power of the light increases, the GST begins to switch from amorphous to crystalline once the temperature exceeds the crystalline temperature T_{crys}. We could simply use CW light as the input to achieve this. In terms of the reverse process, we would not make the GST switch backwards to amorphous state from crystalline state unless we utilize an optical pulse to uproar the medium temperature above to its melting point T_{melt} so that the transition happens during the process of cooling down. In our work, therefore, in seeking of simplicity, for the time being we neither used a pulse signal nor designed a structure for fast thermal dissipation. As a result, we did not take the transition process of from-crystalline-to-amorphous into our consideration and only simulated the amorphous-to-crystalline process in the following work.

Chapter 4. Performance Calculation

In this chapter, we will discuss the performance calculation of our design on optical limiter and show the results of several simulations we performed in this project. To be more specific, we will analyze the thermal distribution of the GST layer in the device and the transmission of the optical limiter using both static and dynamic model. The first work was primarily completed by utilizing the COMSOL simulation software while the latter two models were calculated by using MATLAB. In this work, we made several assumptions regarding the changing process of several optical parameters during the phase transition interval for GST based on already known theories, values and results of simulations.

4.1 Thermal distribution in the GST cavity

As we mentioned above, the phase change of GST happens when the temperature of GST layer goes beyond either the crystallization temperature T_{cry} or the melting temperature T_{melt}. Unlike the approach in a phase change memory that uses an electrical injection to alter the temperature, the input signal for an optical limiter is of course, a CW light. So we need to estimate the temperature of the GST under varying optical intensities. What are the conditions that would make the phase transition happen as smoothly as our expectation? What are the input power and time duration to make an amorphous GST layer transfer to crystalline? To answer these questions, we have to know how the temperature of a GST changes as a function of the input power. Hereby, we need

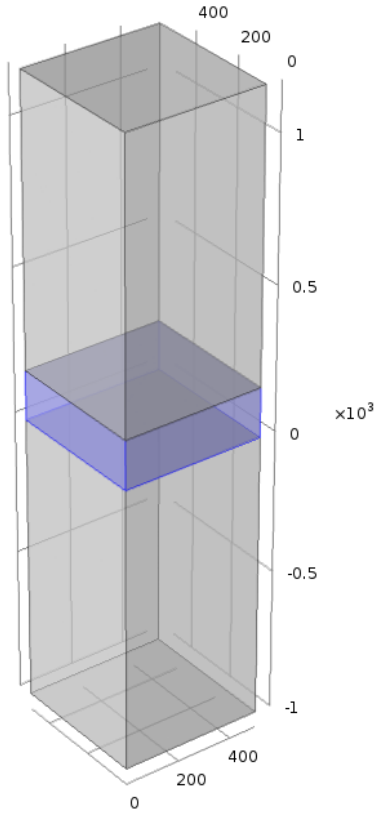

Figure 9 The structure designed for thermal distribution simulation

to have a thermal distribution simulation on our designed device to understand the temperature of the GST inside a cavity and to ensure that it changes as the way we expect, rising above the T_{cry}. In this work, therefore, we utilized COMSOL to perform this simulation on the device's thermal distribution of the GST layer.

To simplify the model of our simulation, we created a structure shown in Figure 9. In this simulation, we mainly focused on the temperature changes in the GST layer according to the injected light that illuminates into the top surface of the GST cavity. Hence we simplified the design of the optical limiter. We replaced the DBR mirrors by two plain Si_3N_4 bulks that sit on both sides of the GST layer with a 500nm×500nm×1000nm dimension for each to form a sandwich structure. The highlighted blue area in Figure 9 is a GST layer. It has the same length and width as the Si_3N_4 bulks, 500nm×500nm and its thickness was set as 171.8nm that would make the center wavelength of the optical limiter at 1550nm. The source of the input light was

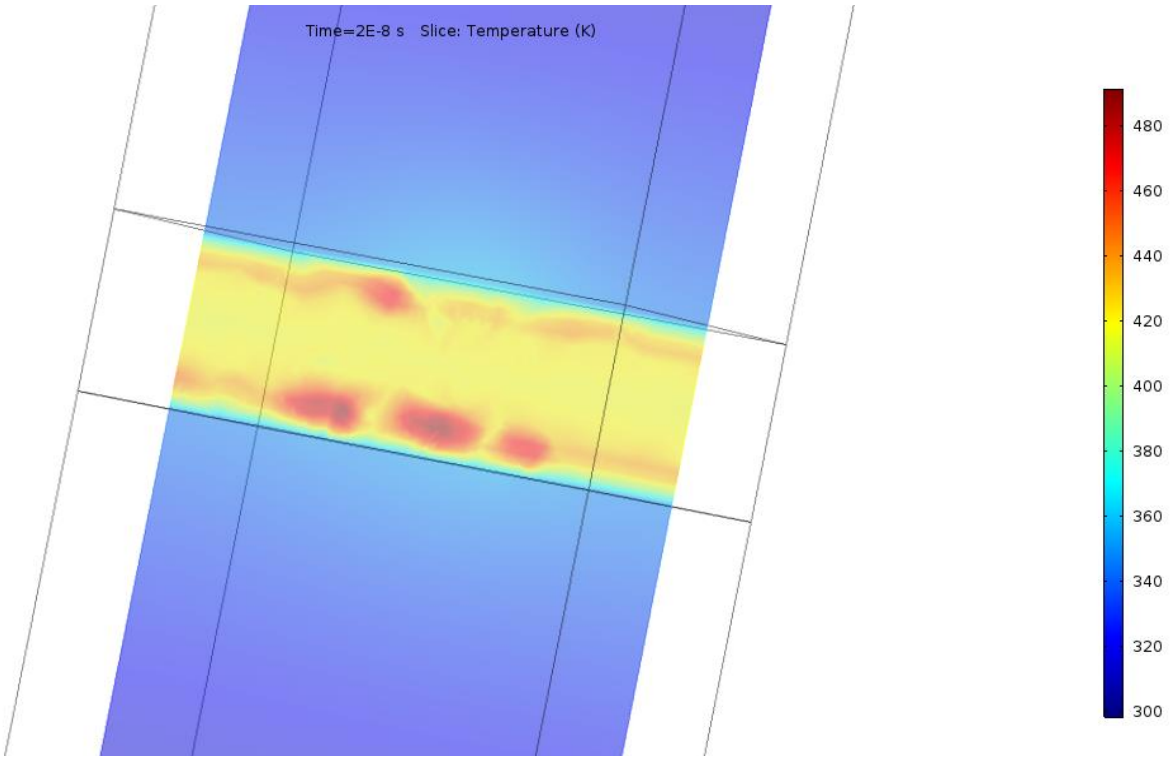

Figure 10 The thermal distribution at 20ns under 10mW

assumed just at the top surface of the GST, shining from top to the bottom. Relative parameters at both amorphous and crystalline states, such as the refractive indices, densities, thermal conductivities, heat capacities were all taken into consideration. Their values at these two states were given by previous works[44]. We used a built-in model, 'Phase Change Material' in COMSOL and set its crystallization temperature T_{cry} at 400K and 10 K of transition interval.

The input power was initially set at 10mW with a 1550nm light and the result of the temperature distribution simulation was shown in Figure 10. It demonstrated that the temperature of most part of the GST layer was just higher than the T_{cry}, 400K, at 20ns under the exposure of 1550nm, 10mW CW light radiation. This suggested that the GST layer just transferred from its amorphous state to crystalline state at 20ns of 10mW input. Hence we regarded this 10mW power as a threshold power P_{th} for a relatively long duration input in the GST layer. We also

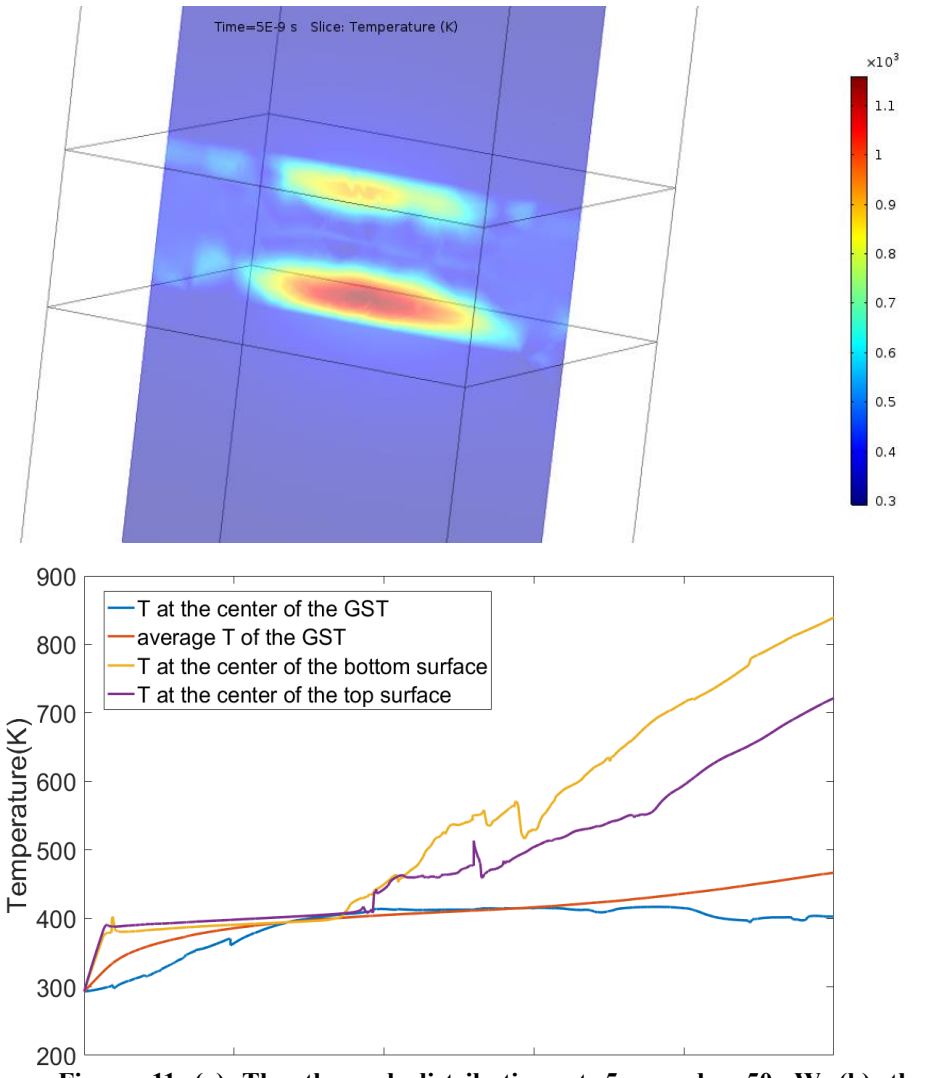

Figure 11 (a) The thermal distribution at 5ns under 50mW (b) the temperature of the three probes during the 5ns radiation

noticed that the temperature distribution in the GST was non-uniform and asymmetrical. The temperature at areas that were close to the top and bottom interfaces were higher than that in the center region. The temperature was highest at the bottom and lowest in the middle of the area. One possible explanation is that due to the reflection at the interfaces, it accumulated more energy, which means higher temperature, around the surface areas. And the GST around the bottom surface may start to transition from amorphous to crystalline state first so the heat capacity and thermal conductivity in that area began to change prior to this happening on the top and middle area. As a result, the thermal conductivity and heat capacity were not uniform during the phase transition and this difference led an unidentical and asymmetrical distribution of the temperature in the GST layer.

In order to understand with more details about the state's transition from amorphous to crystalline, we increased the input power to 50mW to create a more drastic change on the GST's temperature. The result was given in Figure 11. Figure 11a displays the temperature distribution in the layer at 5ns. Almost the entire GST layer's temperature was way above the T_{cry}, 400K at 5ns. We believe that the phase transition of the GST was completed at 5ns and it has been in its crystalline state. The temperature was still highest in the adjacent area of the bottom surface and lowest in the center area of the layer. We think the reason is similar to the case of previous simulations with 10mW input light. We set three point probes inside the GST that located at 10nm above the bottom surface, 10nm below top surface and the center point of the layer. Figure 11b shows the temperature at these probes during this 5ns of light radiation. We found that initially the temperature of each point increased quickly prior to it staying for a period of time at a stable level around 400K, the exact T_{cry}. After this stationary area, the temperature increased once again. The duration of this stable area and the pace of increment were variant for different probes. We believe the phase transition of GST happened exactly at the region where temperature was stable around

400K and the GST was absorbing power dramatically and transferring significantly from amorphous to crystalline within the power range corresponding to this temperature.

According to the discussion above, we made an assumption, that the GST changed from its amorphous state to crystalline state significantly around a certain level of power absorbed by the GST cavity in an optical limiter while the value of its refractive index also had a similar remarkable change within this power interval. According to the thermal distribution simulations above, we assumed this absorbed power was 10mW for a CW input light. We also called it the threshold power or P_{th}=10mW. Since the molecular structure in a GST is relatively stable when its temperature is far below or far beyond the crystallization point. It is reasonable to assume that the refractive index n and k are almost the same as n_{am}(1550nm) and k_{am}(1550nm) when $T<<T_{cry}$ and

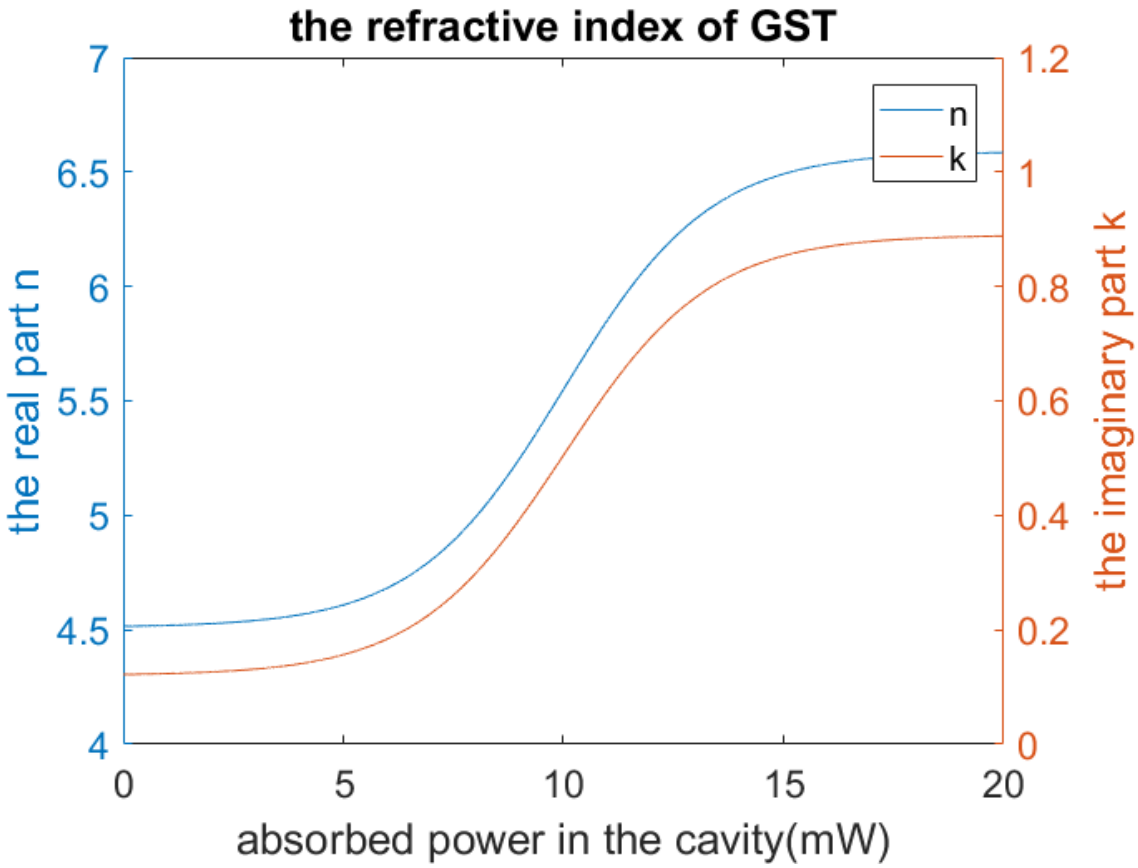

Figure 12 The refractive index as a function of the absorbed power by GST

they are almost the same as n_{cr}(1550nm) and k_{cr}(1550nm) when $T>>T_{cry}$. A significant change

should occur around the crystallization temperature T_{cry}. Combining this relation together, we proposed that the refractive index of the GST n and k were described in equation (12) and (13) as hyperbolic tangent functions of the absorbed power, where η=300/mW represented the strength of the phase change of the GST cavity.

$$n = \frac{n_{am} + n_{cr}}{2} + \frac{n_{am} - n_{cr}}{2} \cdot \tanh\left[\eta\left(P_{abs} - P_{th}\right)\right] \tag{12}$$

$$k = \frac{k_{am} + k_{cr}}{2} + \frac{k_{am} - k_{cr}}{2} \cdot \tanh\left[\eta\left(P_{abs} - P_{th}\right)\right] \tag{13}$$

The relation between the refractive index of the GST and the absorbed power by the cavity was drawn in Figure 12. The value of the coefficient η represents how dramatic the GST's phase transition is. That is to say, the larger value of η, the narrower power window around P_{th} will it have for the GST transferring from one state to the other and the smaller of it, the wider will it appear on change of the refractive index as a function of the absorbed power. In addition, we would like to point out that η=300/mW was only a hypothetical value in our work and the actual value of it needs to be determined by experimentations.

4.2 The static transmissivity in optical limiter

Based on the aforementioned assumptions, we simulate the transmissivity of the optical limiter in a static model. In order to calculate the transmissivity of the optical limiter, we used transfer matrix to calculate the light transmission in a multi-structure device.

Figure 13 displays a basic idea of light traveling through a multi-layer structure. d_1, d_2, and d_3 represent the thickness of film 1, 2 and 3 while n_1, n_2 and n_3 represent their refractive indices, respectively. λ_0 is the wavelength in vacuum of the input light. In thin film transmission theory, the transfer matrix in a single layer can be written in equation (14) and equation (15a) and (15b), where T_2 is the transfer matrix of light propagating in film 2 and T_{12} and T_{23} are the transfer matrixes of the boundary conditions of respectively. $k_1 = \frac{2\pi n_1}{\lambda_0}$, $k_2 = \frac{2\pi n_2}{\lambda_0}$ and $k_3 = \frac{2\pi n_3}{\lambda_0}$ are the propagation constants corresponding to each layer.

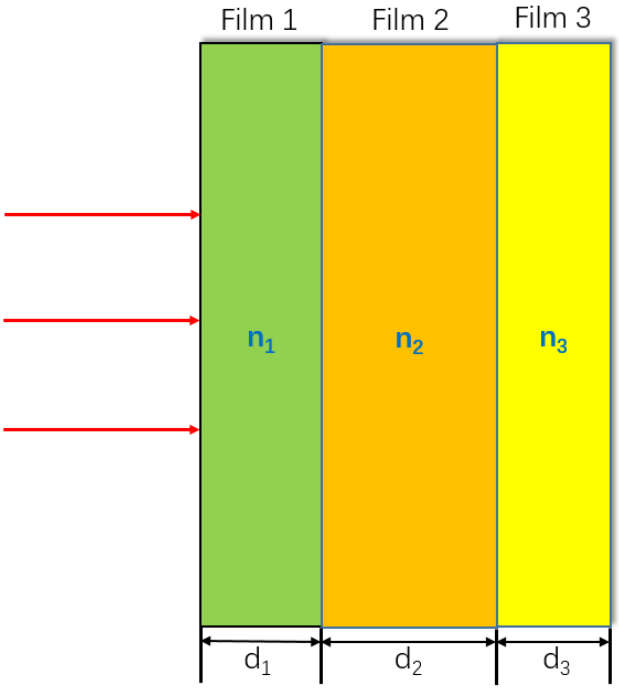

Figure 13 A multilayer structure for light transferring through

$$T_2 = \begin{pmatrix} e^{ik_2 b} & 0 \\ 0 & e^{-ik_2 b} \end{pmatrix} \tag{14}$$

$$T_{12} = \begin{pmatrix} \frac{1+k_2/k_1}{2} & \frac{1-k_2/k_1}{2} \\ \frac{1-k_2/k_1}{2} & \frac{1+k_2/k_1}{2} \end{pmatrix} \qquad T_{23} = \begin{pmatrix} \frac{1+k_3/k_2}{2} & \frac{1-k_3/k_2}{2} \\ \frac{1-k_3/k_2}{2} & \frac{1+k_3/k_2}{2} \end{pmatrix} \tag{15a), (15b)}$$

The transfer matrix of light traveling through film 2 can be written as $M = T_{12}T_2T_{23}$ and the reflectivity and transmittance of film 2 can be represented by equation (16a) and (16b)[45]. We need to point out that equation (16b) is valid only when there is no loss in the device. If we take optical loss into consideration, the transmissivity is then given by equation (16c). By using these

equations and combining the parameters we used for our design, we calculated the reflectivity (transmittance) of the DBR in Figure 4c and plotted the result in Figure 14. For comparison, we also drew in the same plot with the transmissivity of DBRs that have 10 pairs and 2 pairs of the alternating layers. As the figure suggests, choosing only 2 pairs of DBR does not satisfy the requirement for a large reflectivity at center wavelength of the DBR. Although a 10-pairs-DBR has a higher reflectivity, the trade-off is that it would also bring greater difficulties in a real device fabrication. Therefore, we utilized 6 pairs of repeating dielectric layers in our design.

$$R = r^2 = \left|\frac{M(2,1)}{M(1,1)}\right|^2 \tag{16a}$$

$$T_{no\text{-}loss}=t^2=1-R \tag{16b}$$

$$T = t^2 = \left|\frac{1}{M(1,1)}\right|^2 \tag{16c}$$

According to the equations from (14) to (16a) and Figure 12, the reflectivity of the DBR on both sides of GST layer is a function of wavelength. At the designed resonance wavelength, λ=1550nm, the largest reflectivity of the DBR occurs and the exact value of the reflectivity is R(λ=1550nm)=0.95.

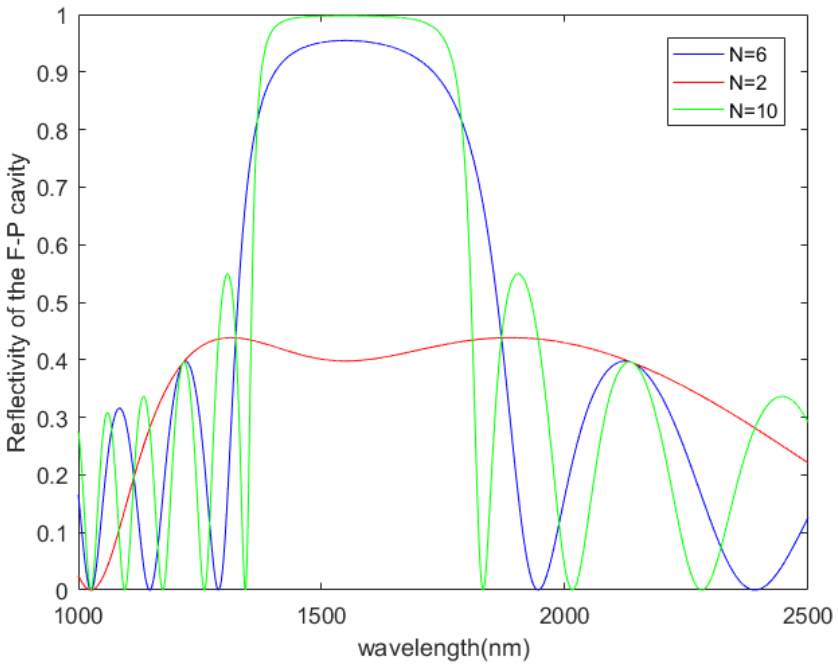

Figure 14 The reflectivity of the DBR we designed

In a DBR-based Fabry-Perot cavity, however, the actual power transmittance of the F-P cavity is more complicated than the relation demonstrated by equations (5) and (6). As

we discussed above, from equation (5) and (6), the transmissivity of the F-P cavity would be also a function of wavelength and there are two contributors, the influences from the reflectivity of the two mirrors on its both sides and the contribution from the phase of the phase change material itself which determines the refractive index of the GST. However, the reflectivity of the mirrors besides the cavity is not the exact reflectivity of the DBR we discussed in Figure 14. This is because the light will penetrate into both DBR for a certain number of layers and involve several layers of the dielectric being coupled with the cavity internal medium, the GST. Hence, when applying equation (5) and (6) to calculate the transmissivity of the limiter, we have to consider the effective thickness of cavity and the effective reflectivity of each DBR mirror.

The transfer matrix method, however, is still valid for the entire limiter regardless of how many layers of the dielectrics are coupled with the cavity. Therefore, we used transfer matrix methodology to establish our static model and calculate the transmissivity of the device.

Combining the F-P cavity and the DBR layers together as a multi-layer system, in Figure 15, we can then have the entire structure of the optical limiter. Assume there is no light actually coming in and the limiter is at its initial (amorphous) state. According to equations from (14) to

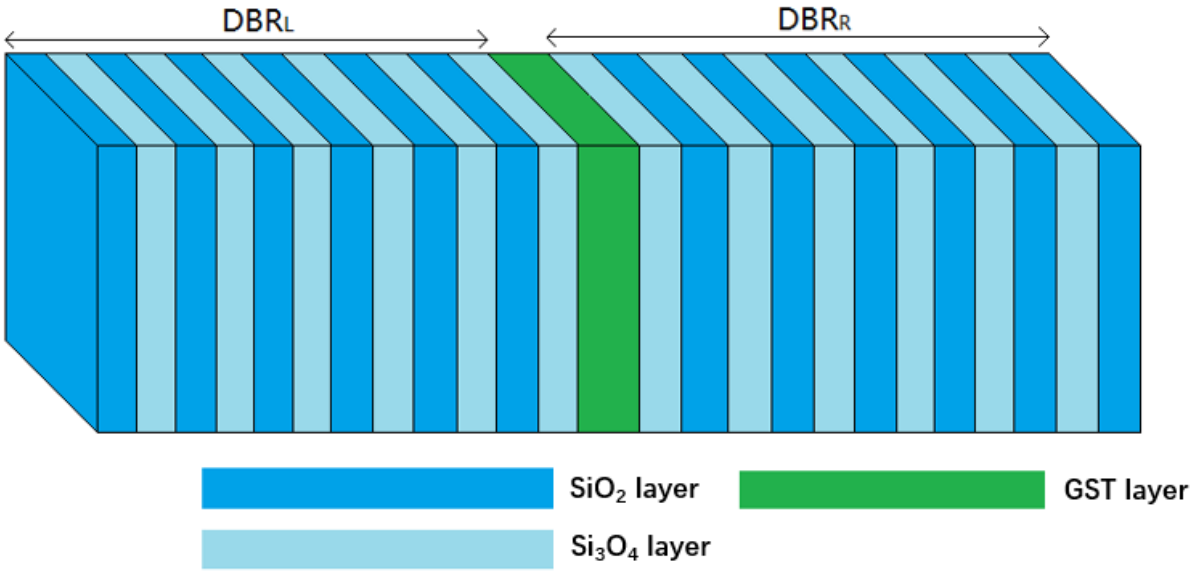

Figure 15 The structure of the entire optical limiter we designed in this work

(16c) for multilayers' light transmission, the transmissivity and the cavity's resonance wavelength of the limiter can be calculated. The result was drawn in Figure 16, in which we assumed that the GST had refractive indices that were independent of the light wavelength. In this simulation, the values of the refractive indices of the GST in both amorphous and crystalline states were given by the data demonstrated in Figure 8, where n(amorphous)=4.506, k(amorphous)=0.124, n(crystalline)=6.594, k(crystalline)=0.895. Considering the feasibility of fabrication and the possible applications of our limiter, we think it would be a reasonable thickness of the GST layer around 200nm. At amorphous(initial) state, therefore, by utilizing MATLAB, we swept the thickness of the GST from 150nm to 250nm and calculated the resonance wavelength. We found that the resonance was exact at 1550nm when the thickness was 171.8nm.

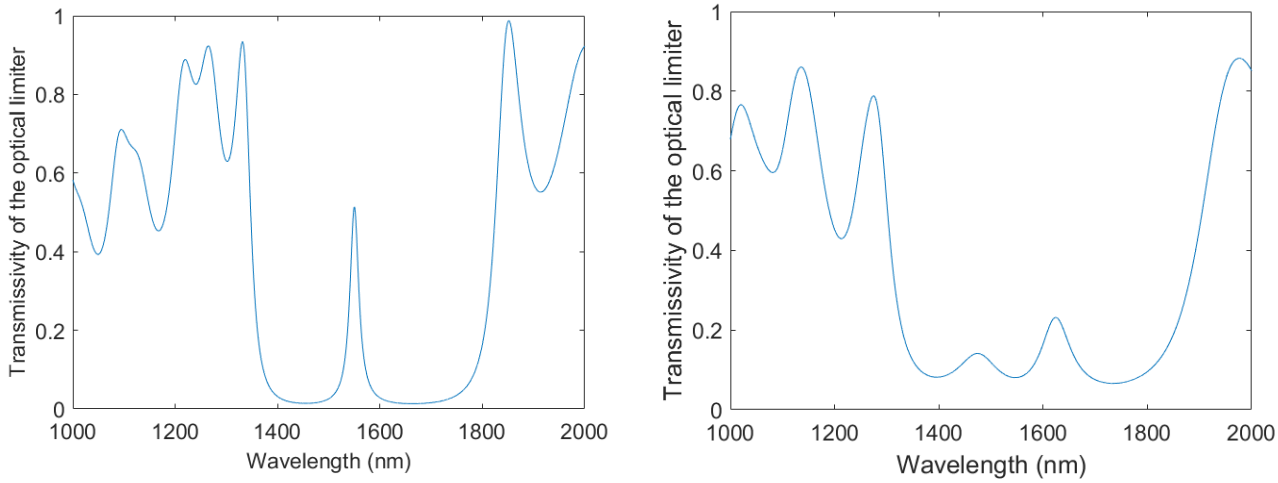

Figure 16 The transmissivity of the optical limiter as a function of wavelength in (a) amorphous state (b) crystalline state when the refractive index is independent of wavelength

In Figure 16a, the transmissivity of the optical limiter was demonstrated as a function of the wavelength while the GST was at the amorphous state. Similarly, if we assume somehow the GST has been transferred into crystalline state from amorphous, then the transmissivity as a function of the wavelength can be plotted in Figure 16b when the refractive indices were fixed at the crystalline level n_{cr} and k_{cr} respectively. Comparing the resonance peaks between Figure 16a and 16b, we

found that the resonance in amorphous state GST cavity lied at 1550nm according to our device design. And the resonance had a significant red shift to the right to 1630nm in crystalized GST cavity which contained higher refractive indices and greater loss than those in amorphous cavity.

In the model above, the refractive indices were assumed to be independent of the wavelength. That is to say, no matter in which state the GST was, the refractive indices in the simulation we conducted above were all fixed at the values that corresponds to the GST's state, though the results we got in Figure 16 were good enough to have a general understanding about how the power transmittance was in our optical limiter. This, however, was not the actual case.

To simulate a more realistic setup, we have to move one step forward. We involved the change of refractive indices as a function of light wavelength and performed the simulation again, the results were represented in Figure 17a and 17b. Similar to Figure 16a and 16b, Figure 17a and 17b demonstrated the transmissivity as a function of wavelength in the cases of both amorphous and crystalline states. According to the results shown in Figure 17a and 17b, we noticed that the T under these two situations were similar to the results shown in Figure 16a and 16b. The resonance of the cavity still located at 1550nm in amorphous state and significantly shifted to 1630nm when

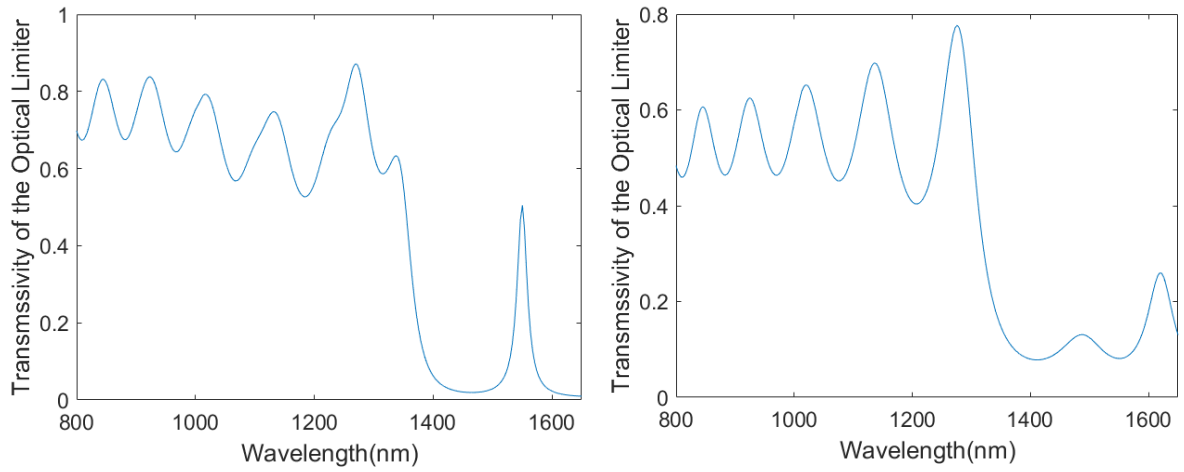

Figure 17 The transmissivity of the optical limiter as a function of wavelength in (a) amorphous state (b) crystalline state when the refractive index is independent on wavelength

the GST was in crystalline. It suggests that the refractive indices' dependence on input wavelengths had little impact on the change on the resonance of the cavity.

Nevertheless, the data of the relation between the refractive indices and wavelength had a wavelength range from around 200nm to 1700nm. But the DBR bandgap of our device was from around 1300nm to 1800nm. It is very difficult to alter the bandgap in this device because based on equation (10), this bandgap range was fixed as long as the refractive index of the dielectric material used for DBR was determined and the center wavelength was selected. In order to have a better understanding about the device performance, especially when the wavelength was beyond 1700nm, in the following simulations, we assumed the refractive indices of GST were independent of the wavelength of input light, and fixed at the values at 1630nm.

According to the assumption we made on the refractive indices as a function of the absorbed power by GST in equation (12) and (13), we could get the refractive indices of GST under variant absorbed powers, 0, 6mW, 10mW, 14mW, 20mW for instance. We used the same way as we did in plotting Figure 16a and 16b to calculate the optical limiter's transmissivity as a function of wavelength under these absorbed powers. The results were given in Figure 18. At initial state, when there was no actual light coming in and P_{abs}=0, the result was the same as we shown in Figure 16a. The GST rested in its

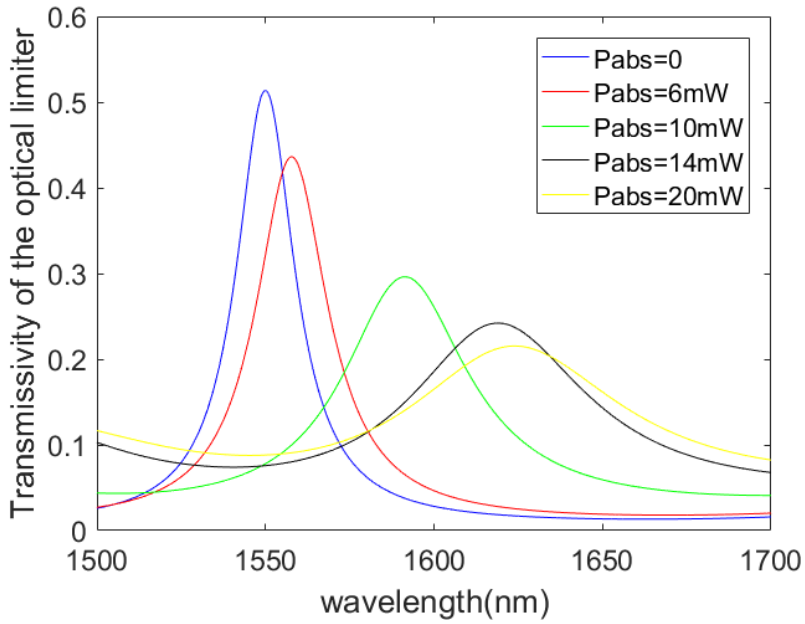

Figure 18 The transmissivity as a function of wavelength under different absorbed power

amorphous state and the resonance was at 1550nm while the transmissivity at this resonance was about 0.5. If there was an incident light, the GST layer started to absorb energy and the temperature rose. The GST's phase was gradually transferred towards crystalline state and so were the refractive indices. Therefore, the resonance of the cavity gradually shifted towards the infrared direction as the increasing of the absorbed power and the refractive indices. Due to the increase on the imaginary part of the refractive index, the cavity loss went up as well, leading to a decrease on the transmissivity at resonance wavelength. In particular, the refractive indices at 0 and 20mW were respectively very close to the values at amorphous state and crystalline state. This is because when the absorbed power was far away from the threshold power P_{th}=10mW, the GST was also away from the transition region and its refractive indices should be either close to the values in amorphous state or those in crystalline state.

At the center wavelength 1550nm, it was suggested in Figure 18 that the transmissivity also had a considerable decrease from 0 to 20mW of the absorbed power. We then calculated the transmissivity of the optical limiter again. But this time we kept the wavelength fixed at 1550nm and swept the absorbed power from 0 to 20mW. The result of this calculation showed the transmissivity as a function of the power absorbed by the cavity at 1550nm and was plotted in Figure 19. The T was at

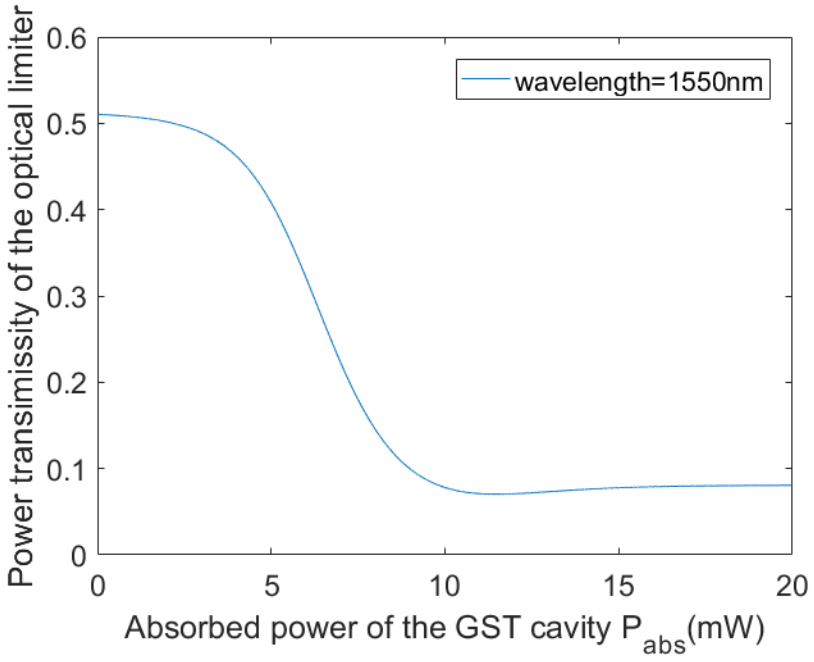

Figure 19 The transmissivity as a function of absorbed power at 1550nm

a high level around 0.5 when the absorbed power was relatively low and the GST should accordingly be at its amorphous state. When the absorbed power went up to the phase transition range, the GST changed significantly and the transmissivity dropped drastically in this interval too. When the phase transition was almost complete, the transmissivity reached its bottom value and stayed at the low level regardless how much more power the GST would absorb. Based on our design and calculations so far, we successfully got considerably different transmissivities at two phase states and a nonlinear transition process between them in accordance to the absorbed power. This is very promising for this optical limiter based on phase change material.

4.3 The dynamic transmissivity in optical limiter

To understand the most realistic situation, it is necessary to develop a dynamic model. So far we have discussed the static model of the optical limiter and analyzed the power transmittance of the optical limiter when the absorbed power was given at a specific level. Things become more complex if we apply a continuous incident light at the input port of the optical limiter. According to aforementioned discussion in Figure 16, the increase of absorbed power would make the transmissivity go down and raise the cavity loss of the device. And the increase of cavity loss would in turn to furtherly lower the transmissivity. There was a positive feedback mechanism in the cavity until the transition of the GST's phase was completed. We built a dynamic model in measuring this case so that we could have the relation between the output power as a function of the input power of the device as well as the transmissivity as a function of the input power.

For a dynamic model of a GST cavity, the electrical field of the cavity can be expressed in equation (17)[46] when it is driven by an external laser radiation, where Δ is the detuning of the angular frequency from the cavity resonance, γ_c and γ_{abs} represent the field decay rate of the cavity while the former one is caused by coupling to the outside cavity and the latter one is because of

the absorption of the cavity. At same time, the amplitude of the output light of the cavity and the absorbed by the F-P cavity are able to be described in equation (18) and (19) respectively.

$$\frac{dE(t)}{dt} = i\Delta \cdot E(t) - (\gamma_c + \gamma_{abs}) \cdot E(t) + i\sqrt{2\gamma_c} \cdot S_{in} \tag{17}$$

$$S_{out} = S_{in} + i\sqrt{2\gamma_c} \cdot E \tag{18}$$

$$S_{abs} = i\sqrt{2\gamma_{abs}} \cdot E \tag{19}$$

Considering the relation between the amplitude and the power of the light, we have $P_{in} = |S_{in}|^2$, $P_{out} = |S_{out}|^2$ and $P_{abs} = |S_{abs}|^2$. Substituting equation (17)-(19) into them, some groups described the relation between the input power into the GST cavity and the absorbed power of the cavity in equation (20) by letting $\Delta = \Delta_0 + \mu P_{abs}$, where Δ_0 is the initial detuning angular frequency[46, 47].

$$\mu^2 P_{abs}^3 + 2\mu\Delta_0 P_{abs}^2 + \left[(\gamma_c + \gamma_l)^2 + \Delta_0^2\right] P_{abs} = 4\gamma_c \gamma_l P_{in} \tag{20}$$

But equation is not valid in our project because the detuning is no longer a linearly parameter in this work. Actually, we need to know the initial and final values of γ_c, γ_l, detuning Δ to determine the absorbed power with a given input power. The absorbed power in turn affects the transition of the state in the GST as well as the refractive indices n and k, detuning Δ, γ_c, γ_{abs} and thus, of course, the transmissivity T. When these parameters are altered, the absorbed power changes again and modifying all the cavity parameters. This occurs again and again in the GST cavity so we had to establish a dynamic model to do the analysis of the power transmittance of the optical limiter.

The input light is at 1550nm, the center wavelength. In this dynamic simulation, the initial and the final values of γ_c were set as $2\pi\times8$THz and $2\pi\times36$THz respectively while those values of the γ_{abs} were $2\pi\times36.5$THz and $2\pi\times77.5$THz. Similar to the assumptions we made for the transition of refractive index of the GST, we utilized equation (21) and (22) to describe the relation of γ_c and

γ_{abs} according to the value of absorbed power, where γ_{c0} and γ_{c1} correspond to the field decay rate by coupling at amorphous state and crystalline state respectively while γ_{abs0} and γ_{abs1} correspond to those of the field decay rate by absorption. The values of γ_c and γ_{abs} as a function of absorbed power were plotted in Figure 20.

$$\gamma_c = \frac{\gamma_{c1}+\gamma_{c0}}{2} + \frac{\gamma_{c1}-\gamma_{c0}}{2} \cdot \tanh\left[\eta\left(P_{abs}-P_{th}\right)\right] \tag{21}$$

$$\gamma_{abs} = \frac{\gamma_{abs1}+\gamma_{abs0}}{2} + \frac{\gamma_{abs1}-\gamma_{abs0}}{2} \cdot \tanh\left[\eta\left(P_{abs}-P_{th}\right)\right] \tag{22}$$

The shape of the curves in Figure 20 was similar to that of the refractive indices' curve as a function of the absorbed power. This was not beyond expectation because we assumed that they all obeyed the hyperbolic tangent relation with the cavity absorption and they had remarkable changes within the phase transition interval, especially when absorbed power was close to the threshold power P_{th}=10mW.

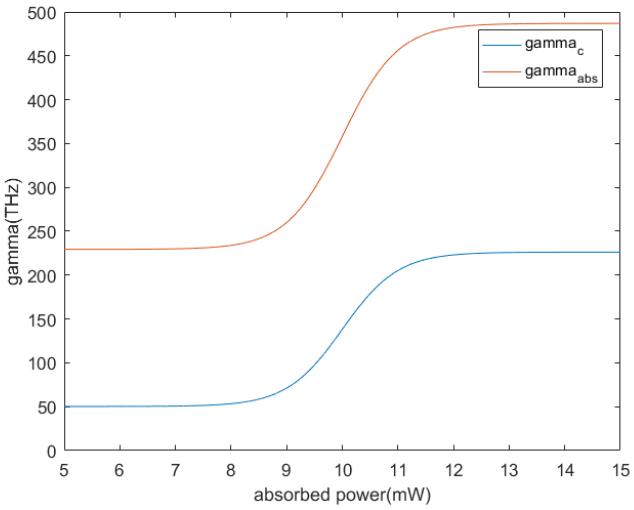

Figure 20 The coupling coefficient as a function of absorbed power

We also calculated the resonance and detuning of the limiter based on previous static modeling. We assumed there was no loss in the GST cavity and got rid of the imaginary part of the refractive index. Then again, we calculated the transmissivity as a function of wavelength under different absorbed power in the same way we performed in plotting Figure 16 (except that this time we set k=0 for all absorbed powers). The results were drawn in Figure 21a, from which we could clearly see the 5 resonances of the cavity at P_{abs}=0, 6mW, 10mW, 14mW and 20mW

respectively. Hence, it was possible to find the resonance of the F-P cavity as well as the detuning Δ as a function of absorbed power. We swept the absorbed power from 0 to 20mW and extracted the positions of the resonance at each P_{abs}. The relation was plotted in Figure 21b.

By applying the results we simulated for γ_c, γ_{abs} and the detuning Δ into equation (17), (18), and (19) and taking the DBRs on both sides into calculation, we measured the relation between the total input power P_{in} and the total output power P_{out}. The power of the input light P_{in} represented the total light power that was injected from the very input port of the designed optical limiter and P_{abs} represented the power absorbed by the GST layer in the F-P cavity. We swept the P_{in} from 0 to 500mW in MATLAB and made the grids of P_{in} small enough so that they were reasonable to represent the first order deferential of P_{in} in MATLAB. Solving the equations (17), (18), and (19). The result of the total output power of the limiter P_{out} was plotted in Figure 22a. We also calculated the absorbed power P_{abs} as a function of the total input power P_{in} and drew the plot in the same figure.

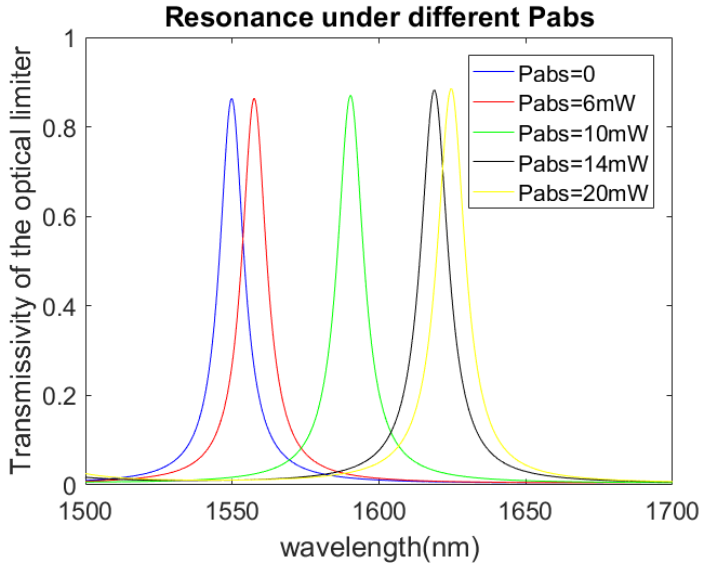

Figure 21a The T as function of wavelength under different wavelength when k=0

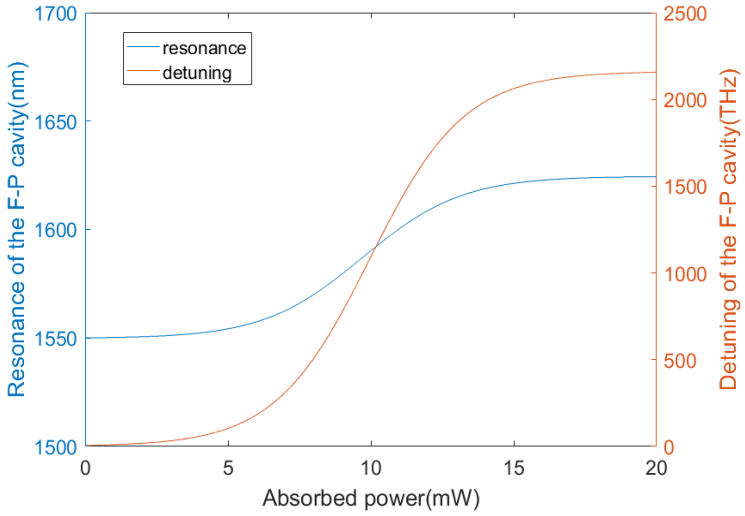

Figure 21b The resonance and detuning as a function of the absorbed power

Figure 22a demonstrated a remarkable nonlinearity of the GST

in the optical limiter that led to a strong nonlinear absorption. We noticed that at low input light intensity range, the output power of the optical limiter had almost a linear relation with the input power. This is because at low input power P_{in}<70mW, the absorbed power by the GST was relatively small at P_{abs}<5mW. The radiation was not sufficient enough to heat the GST up to its crystalline temperature. At this stage, the transmission T did not have a dramatic change in response to the change on input power. T was also stable but relatively low within a high level of input radiation, P_{in}>120mW, where the radiation was strong enough to make the GST complete its transition to crystalline state. At this stage, the T was much lower than that at low level input range and the proportion of the transmitted light was very small. Therefore, at these two areas, the transmission T could be regarded as a constant and the output increased almost proportionally with the rising of input power though the latter one was at a much slower pace.

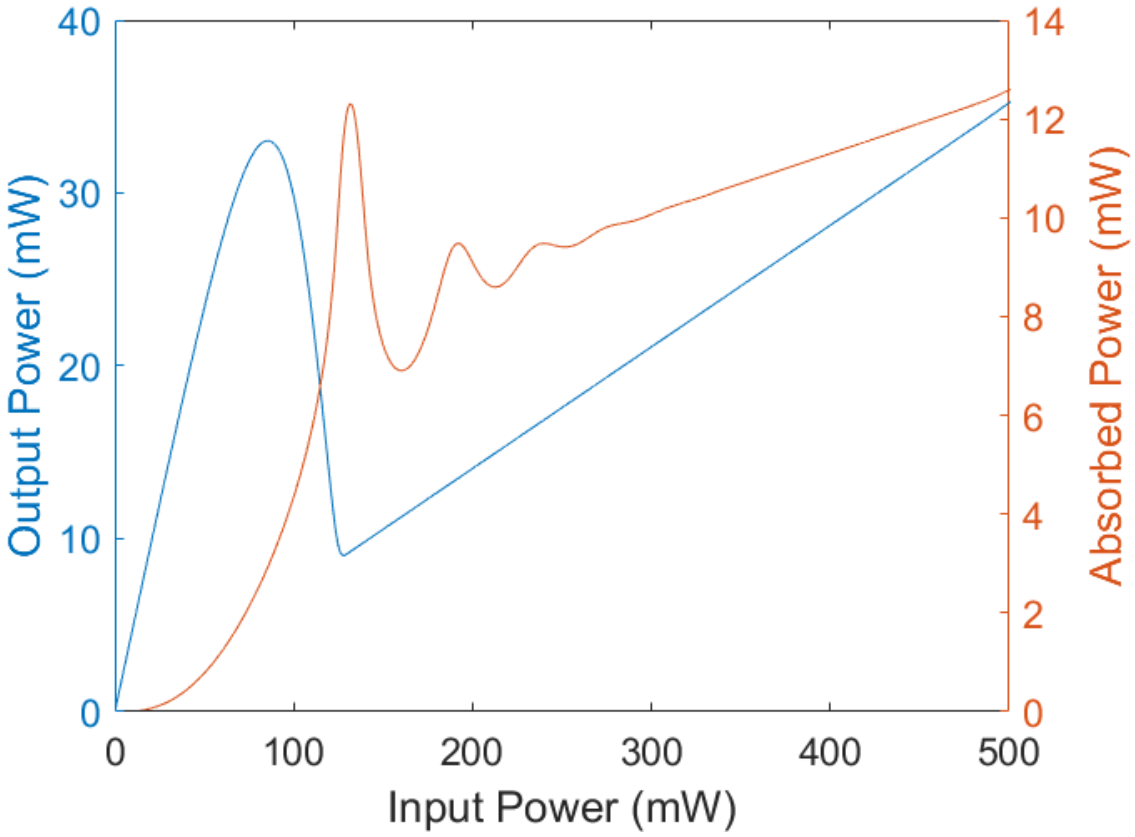

Figure 22a The output power and the absorbed power as a function of the total input power

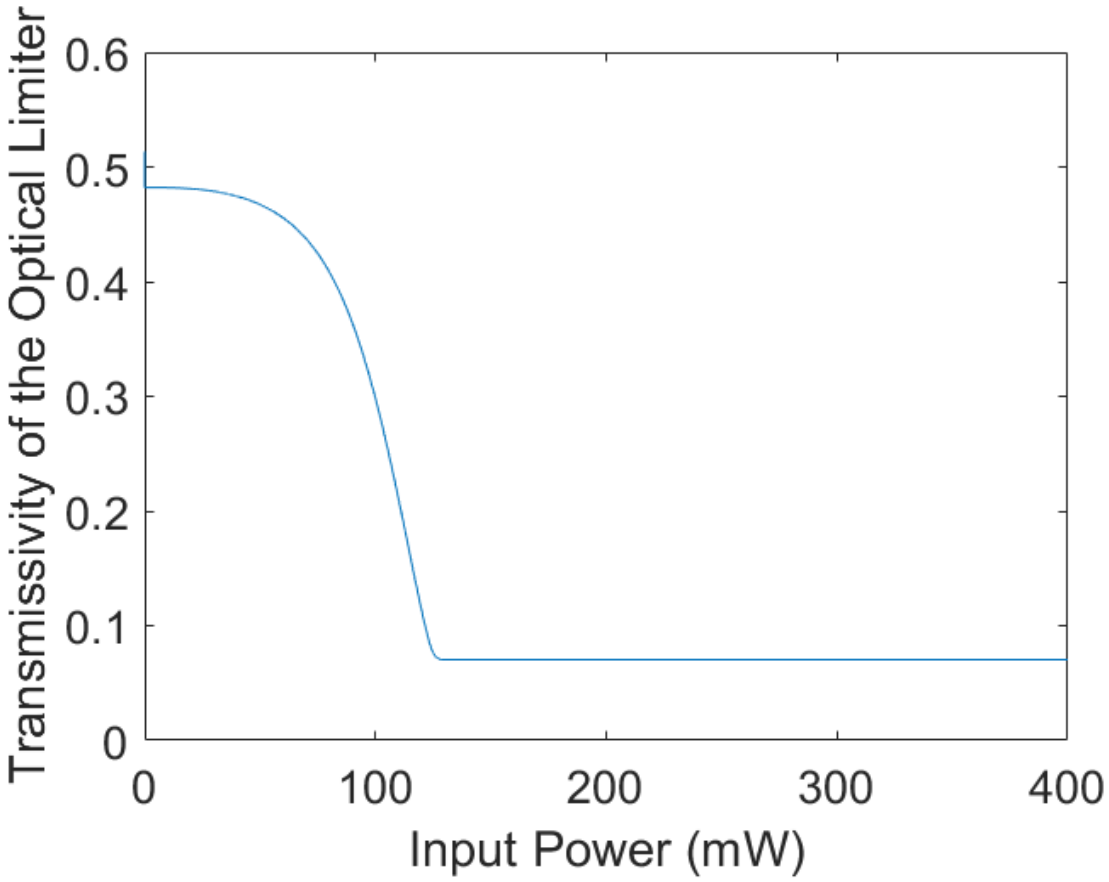

Figure 22b The transmissivity as a function of the total input power

When the absorbed power was closer to the power threshold, P_{th}=10mW in our simulation, the GST layer was expected to switch from amorphous to crystalline, especially when P_{abs} was in the transition interval. Once the absorption entered the transition area, related parameters (n, k, γ_c, γ_{abs}, Δ) started to change drastically. As the result of this phase altering, the transmissivity T of the GST cavity dropped dramatically. In order to have a better understanding on the transmissivity of the entire limiter as a function of the total input power, the relation between them was calculated and drawn in Figure 22b. Therefore, the entire GST optical limiter became less transparent and the device was functional and partially blocked light as expected. Accordingly, becoming less transparent indicated that the GST layer would absorb more energy so the absorbed power had an exponential increase in the phase transition region. The range of the input power for this region was 70mW<P_{in}<120mW, as shown in both Figure 22a and 22b.

This phenomenon corresponds to the assumption in equation (21) and (22) that increasing the absorbed power increases both cavity coupling and cavity absorption γ_c, and γ_{abs}. If the intensity of the input radiation keeps going up, however, the GST layer will be completely transferred into its crystalline state. After this transition region, the change of the refractive indices and loss of the cavity slows down gradually. Raising the absorbed power does not help to further lower the transmission of the device. Hence, the output power of the optical limiter goes up accordingly to the increase of the input power again while the rate of the increment is lower than that at the amorphous state.

In particular, we need to emphasis that the phase change of GST is a one-way process as long as the temperature of the device is lower than the melting temperature. The phase stays at crystalline state as long as the transition is completed. In Figure 20a and 20b, the GST would almost be in crystalline state once the absorbed power P_{abs} was about 12mW when P_{in} was around 120mW. There was no going-back for the transmissivity of the optical limiter even though there were fluctuations of the absorbed power when the input power was greater than 120mW.

Chapter 5. Conclusions

In this project, we demonstrated a design of an optical limiter based on phase change material. By utilizing a Fabry-Perot interferometer and two DBR mirrors, we successfully created a cavity which becomes a key component for the optical limiter design. The device was mainly designed for infrared input radiation, specifically with its center wavelength at 1550nm. Initially, the optical limiter was set at amorphous state whose resonance is at 1550nm. According to the assumption we made for the state transition region, the device demonstrated an impressive light limiting effects. The increase of input intensity of laser radiation at the initial stage of high level power transmittance led to the absorbed power and output power both going up. As the gradual increasing of absorbed power of the GST cavity, the temperature of the F-P cavity rose and when the temperature reached into the state transition area, the molecular structure of the GST changed dramatically towards crystalline state. Relative parameters, therefore, also had significant changes from their amorphous state values to crystalline state values. Typically, the transmissivity dropped drastically during the change. Hence we had an obvious decrease of the output intensity at an input range from 70mW to 120mW. This corresponded to the second case we discussed at the very beginning of this paper, shown in Figure 2b. Even though the output light continued to increase after around 120mW of the input power, the increment of the output power was much slower than its previous level thanks to the low transmissivity at crystalline state. This was the scenario 3 we discussed in Figure 2b.

However, there is still a lot of room for improvements and there are more works needed to verify our assumptions. A very straight-forward way is to fabricate an actual optical limiter device according to the design. Then we need to conduct real experiments on a real device to check whether or not it matches with the model we established so far. Particularly, we want to check if

we had a reasonable assumption on the values of coefficient η, threshold light power P_{th}. In addition, in this simulation, we discussed the device's transition process from amorphous to crystalline only. Therefore, we will still have to propose reasonable methods or revise our design to simulate the reverse process, from crystalline to amorphous. Thus a power bi-stability of the device could be established.

Generally speaking, although a lot of work is still in need ahead, we demonstrated in this work a feasible design of an optical limiter. The simulation results of the design were very promising that suggested a great potential of future applications, such as protection devices for photon detectors, photonic integrated circuits or other optical sensitive micro devices. As long as the device fabrication is completed and actual experiments are conducted, we may be able to establish more practical models in describing the relation between the output power and the input power of the device. Then a revised design of optical limiter can be fabricated and used into real applications in protecting objects from being damaged by high laser illumination.

Acknowledgement

I would like to give my greatest appreciation to my advisors Prof Arka Majumdar and Prof Lih Lin who offered me great supports and guidance during not only in this Master research project but also in my entire graduate program. Especially I would like to thank Prof Majumdar, without whom I could not possibly finish this research to the way it is right now. He gave me a lot of help with his great patience that made me understand a lot in this field and move forward. I also like thanks University of Washington for providing me a such wonderful opportunities and resources to help me successfully complete my program and this advanced graduate degree. I am grateful as well to my lab-mates Jiajiu, Yueyang, Chuchuan, Taylor, Shane and Alan for their generosity in giving me many suggestions on my project.

References

1. Kahn, L.M., *Optical power limiting in multilayer systems with nonlinear response.* Physical Review B - Condensed Matter and Materials Physics, 1996. **53**(3): p. 1429-1437.
2. Liu, X., J.W. Haus, and M.S. Shahriar, *Optical limiting in a periodic materials with relaxational nonlinearity.* Optics express, 2009. **17**(4): p. 2696.
3. Miroshnichenko, A.E., I. Pinkevych, and Y.S. Kivshar, *Tunable all-optical switching in periodic structures with liquid-crystal defects.* Optics Express, 2006. **14**(7): p. 2839-2844.
4. Soon, B.Y., et al., *One-dimensional photonic crystal optical limiter.* Optics Express, 2003. **11**(17): p. 2007-2018.
5. Vella, J.H., et al., *Experimental Realization of a Reflective Optical Limiter.* Physical Review Applied, 2016. **5**(6): p. <xocs:firstpage xmlns:xocs=""/>.
6. Zeng, Y., X. Chen, and W. Lu, *Optical limiting in defective quadratic nonlinear photonic crystals.* Journal of Applied Physics, 2006. **99**(12).
7. Hadhazy, A., *How it works: NASA's Experimental Laser Communication System.* Popular Mechanics.
8. David, L., et al., *Laser abrasion for cosmetic and medical treatment of facial actinic damage.* Cutis, 1989. **43**(6): p. 583-587.
9. Lennox, C.D. and S.P. Beaudet, *Medical treatment of deeply seated tissue using optical radiation*. 1995, Google Patents.
10. Dye, R.A. and D.A. Rowley, *Laser weapon simulator*. 1976, Google Patents.
11. Guoguang, R., *Current Situation and Development Trend of High Energy Laser Weapon [J].* Laser & Optoelectronics Progress, 2008. **9**: p. 013.
12. Sepp, G., *Laser weapon system*. 1997, Google Patents.
13. Waynant, R.W. and R.C. Elton, *Review of short wavelength laser research.* Proceedings of the IEEE, 1976. **64**(7): p. 1059-1092.
14. Cao, X., et al., *A review of laser welding techniques for magnesium alloys.* Journal of Materials Processing Technology, 2006. **171**(2): p. 188-204.
15. Commission, I., *Safety of laser products–Part 1: Equipment classification and requirements. IEC 60825-1*. 2001, International Electrotechnical Commission: Geneva.
16. Bader, O. and H. Lui. *Laser safety and the eye: hidden hazards and practical pearls*. in *American Academy of Dermatology Annual Meeting Poster Session, Washington, DC, USA*. 1996.
17. Martinez, L., *Navy's New Laser Weapon Blasts Bad guys from Air, Sea, Yahoo.* News, Apr, 2013. **8**.
18. Bechtel, J. and W.L. Smith, *Two-photon absorption in semiconductors with picosecond laser pulses.* Physical Review B, 1976. **13**(8): p. 3515.
19. He, G.S., et al., *Two-photon absorption and optical-limiting properties of novel organic compounds.* Optics Letters, 1995. **20**(5): p. 435-437.
20. Boggess, T.F., et al., *Nonlinear-optical energy regulation by nonlinear refraction and absorption in silicon.* Optics letters, 1984. **9**(7): p. 291-293.
21. Husaini, S., et al., *Broadband saturable absorption and optical limiting in graphene-polymer composites.* Applied Physics Letters, 2013. **102**(19): p. 191112.

22. Henari, F.Z. and P. Patil, *Nonlinear optical properties and optical limiting measurements of {(1Z)-[4-(Dimethylamino) Phenyl] Methylene} 4-Nitrobenzocarboxy Hydrazone Monohydrate under cw laser regime.* Optics and Photonics Journal, 2014. **2014**.
23. Pawar, S., et al., *Optical Limiting in Nonlinear Fiber Bragg Grating.* Journal of Nonlinear Optical Physics & Materials, 2012. **21**(02): p. 1250017.
24. Tutt, L.W. and T.F. Boggess, *A review of optical limiting mechanisms and devices using organics, fullerenes, semiconductors and other materials.* Progress in quantum electronics, 1993. **17**(4): p. 299-338.
25. Soref, R., et al., *Electro-optical switching at 1550 nm using a two-state GeSe phase-change layer.* Optics express, 2015. **23**(2): p. 1536-1546.
26. Ríos, C., et al., *Integrated all-photonic non-volatile multi-level memory.* Nature Photonics, 2015. **9**(11): p. 725-732.
27. Liang, H., et al., *Simulations of Silicon-on-Insulator Channel-Waveguide Electrooptical 2× 2 Switches and 1× 1 Modulators Using a ${\ bf Ge_2}{\ bf Sb_2}{\ bf Te_5} $ Self-Holding Layer.* Journal of Lightwave Technology, 2015. **33**(9): p. 1805-1813.
28. Hendrickson, J., et al., *Electro-optical 1 x 2, 1 x N and N x N fiber-optic and free-space switching over 1.55 to 3.0 µm using a Ge-Ge 2 Sb 2 Te 5-Ge prism structure.* Optics express, 2015. **23**(1): p. 72-85.
29. Fabry, C. and A. Perot, *Theorie et applications d'une nouvelle methode de spectroscopie interferentielle.* Ann. Chim. Phys, 1899. **16**(7): p. 115.
30. Perot, A. and C. Fabry, *On the application of interference phenomena to the solution of various problems of spectroscopy and metrology.* The Astrophysical Journal, 1899. **9**: p. 87.
31. Song, W., et al., *Refractive index measurement of single living cells using on-chip Fabry-Pérot cavity.* Applied physics letters, 2006. **89**(20): p. 203901.
32. Hecht, E., *Optics 2nd edition.* Optics 2nd edition by Eugene Hecht Reading, MA: Addison-Wesley Publishing Company, 1987, 1987. **1**.
33. Bragg, W.H. and W.L. Bragg, *The reflection of X-rays by crystals.* Proceedings of the Royal Society of London. Series A, Containing Papers of a Mathematical and Physical Character, 1913. **88**(605): p. 428-438.
34. Sheppard, C., *Approximate calculation of the reflection coefficient from a stratified medium.* Pure and Applied Optics: Journal of the European Optical Society Part A, 1995. **4**(5): p. 665.
35. Osting, B., *Bragg structure and the first spectral gap.* Applied Mathematics Letters, 2012. **25**(11): p. 1926-1930.
36. Achtenhagen, M., et al., *Spectral properties of high-power distributed bragg reflector lasers.* Journal of Lightwave Technology, 2009. **27**(16): p. 3433-3437.
37. Pedrotti, F.L. and L.S. Pedrotti, *Introduction to optics 2nd edition.* Introduction to Optics 2nd Edition by Frank L. Pedrotti, SJ, Leno S. Pedrotti New Jersey: Prentice Hall, 1993, 1993.
38. Kischkat, J., et al., *Mid-infrared optical properties of thin films of aluminum oxide, titanium dioxide, silicon dioxide, aluminum nitride, and silicon nitride.* Applied optics, 2012. **51**(28): p. 6789-6798.
39. Ohno, T., et al., *Application of DBR mode-locked lasers in millimeter-wave fiber-radio system.* Journal of lightwave technology, 2000. **18**(1): p. 44.

40. Wong, H.-S.P., et al., *Phase change memory.* Proceedings of the IEEE, 2010. **98**(12): p. 2201-2227.
41. Lai, S. *Current status of the phase change memory and its future*. in *Electron Devices Meeting, 2003. IEDM'03 Technical Digest. IEEE International*. 2003. IEEE.
42. Liu, J., et al., *A multi-scale analysis of the crystallization of amorphous germanium telluride using ab initio simulations and classical crystallization theory.* Journal of Applied Physics, 2014. **115**(2): p. 023513.
43. Morales-Sanchez, E., et al., *Determination of the glass transition and nucleation temperatures in Ge 2 Sb 2 Te 5 sputtered films.* Journal of applied physics, 2002. **91**(2): p. 697-702.
44. Battaglia, J.-L., et al., *Thermal characterization of the Si O 2-Ge 2 Sb 2 Te 5 interface from room temperature up to 400° C.* Journal of Applied Physics, 2010. **107**(4): p. 044314.
45. Choy, H.K.H., *Design and fabrication of distributed Bragg reflectors for vertical-cavity surface-emitting lasers*. 1998, Citeseer.
46. Majumdar, A. and A. Rundquist, *Cavity-enabled self-electro-optic bistability in silicon photonics.* Optics letters, 2014. **39**(13): p. 3864-3867.
47. Fryett, T.K., C.M. Dodson, and A. Majumdar, *Cavity enhanced nonlinear optics for few photon optical bistability.* Optics express, 2015. **23**(12): p. 16246-16255.